CHAPTER 10

Computational investigation on the impact of mutations in the SARS-CoV-2 spike RBD region of BA.2.12.1 and BA.4 variants on its interaction with ACE2 Receptor Protein

Computational investigation on the impact of mutations in the SARS-CoV-2 spike RBD region of BA.2.12.1 and BA.4 variants on its interaction with ACE2 Receptor Protein

10.1. Abstract:

SARS-CoV-2 is an ongoing pandemic due to mutations in the Spike protein giving rise to multiple lineages and sub-lineages with due course of time. The spike protein plays a major role in receptor recognition and cell entry with the help of ACE2 receptor protein. Since the immune evasion mechanism has developed, mutations in the RBD region have resulted in increased infectivity and posed a serious threat. Along with the lineage of Omicron, the pathogenicity of several other omicron sub-lineages, including BA.4, BA.2, BA.2.12.1, BA.5, and others, has increased. BA.2.12.1 and BA.4 shares almost 31 common mutations with BA.2. This study involves physiochemical, structural characterisation and binding properties of the spike protein of BA.4 and BA.2.12.1 variants using various online tools, MD simulation and other computational approaches. Based on the docking studies, BA.2.12.1 is found to be more stable than BA.4 on binding with ACE2 receptor. It has been found that BA.2.12.1 (ΔG_{bind} = -16.65 kcal/mol) has a higher binding affinity than BA.4 (ΔG_{bind} = -4.53 kcal/mol) with ACE2 according to calculations of binding free energy using the MM-GBSA approach. The overall stability of the BA.2.12.1 strain may make it more virulent than the BA.4 type strain.

10.2. Introduction:

Coronaviruses are lipid membrane-encapsulated viruses that are produced from the host cell, and they contain viral surface proteins inside. The genome of each corona strain is a single-stranded RNA with positive polarity and a base sequence that is oriented in the 5′–3′ direction [1]. Viral infections and contagious diseases pose a serious danger to population control and that is due to their error-prone (RdRp) RNA-dependent RNA polymerase, which is responsible for duplicating genetic material and homologous recombination [2]. Since then, numerous mutations have taken place, resulting in multiple strains of SARS-CoV-2, including Alpha (B.1.1.7 lineages), Beta (B.1.351 lineages), Gamma (P.1 lineages), Delta (B.1.617.2 lineages), Lambda variant (C.37), Mu variant (B.1.621) Epsilon (B.1.427 and B.1.429), Eta (B.1.525), Iota (B.1.526), Kappa (B.1.617.1) 1.617.3, Mu (B.1.621, B.1.621.1), Zeta (P.2), Omicron (B.1.1.529, BA.4, BA.4.1, BA.2, BA.3, BA.4 and BA.5 lineages) [3-5].

Angiotensin converting receptor 2 (ACE2) is used by SARS-CoV-2 spike protein to bind and penetrate the human cells. ACE2 is located on cell layers that have a trans membrane anchor and an extracellular domain. [6, 7]. The SARS-CoV-2 Spike protein with a total length of 1273 amino acids comprises of a signal peptide (1–13) at the N-terminal, the S1 subunit (1–14) and the S2 subunit (686–1273). The combination peptide (788–806), heptapeptide rehash succession 1 (HR1) (912–984), HR2 (1163–1213), TM region (1213–1237), and cytoplasm space (1237–1273) comprises of the S2 subunit. The N-terminal domain (14–305) and receptor binding domain (RBD, 319–541) have been identified in the S1 subunit [8, 9]

The Omicron variants include more than 30 mutations on the spike protein, 26 of which are unique to the spike protein and isn't observed in any other strains like Alpha, Beta, Gamma, or Delta, giving it the potential to escape the immune system [10-12]. The omicron variant is a family which consists of multiple sub-lineages such as BA.4, BA.2, BA.3, BA.2.12.1, BA.4 and BA.5 wherein BA.2.12.1 and BA2.12.1 differ in 2 mutations, BA.2, BA.4, and BA.5 differ only in 1 deletion mutation and 3 substitution mutations.

Computational analysis suggests that binding of SARS-CoV-2 variants with human ACE2 enhances its binding ability, which is due to the specific mutations in RBD [13-17]. Mutations in BA.2.12.1 spike protein include 33 mutations, BA.4 with 32 mutations and BA.5 consists of 33 mutations with most significant substitution mutation of L452Q, S704L in BA.2.12.1, L452R, F486V and deletion mutation 69-70 in BA.4 [18]. The L452R and L452Q mutation, one of the most frequent mutations, is the only RBD domain mutation has been associated with increase in SARS-CoV-2 fusogenicity and viral infectivity and this mutation also strengthened the high infectivity by improving the cleavage of the spike protein [19]. In this study, we have compared and evaluated the molecular interactions, effects of mutations on the structural stability and binding properties of the Spike protein (S protein) and ACE2 receptor for the sub-variants BA.2.12.1 and BA.4 using modeling and docking server as well as molecular modeling and other computational approaches.

10.3. Materials and Methods:

10.3.1. Preparation of initial structures and docking.

In order to obtain the 3-D structure of the SARS-CoV-2 receptor-binding domain of BA.4 and BA.2.12.1, we first downloaded the 3-D structure of SARS-CoV-2 S receptor-binding domain bound with ACE2 (S protein-ACE2) (PDB ID: 6LZG with a resolution of 2.50 Å from the Research Collaboratory for Structural Bioinformatics Protein Data bank (www.rcsb.org) [20] and separated

out the RBD of S protein and the variant structures were obtained by inducing punctual mutation in the RBD using UCSF Chimera package alpha v.1.12 [21]. The punctual mutations induced in the 6LZG to construct the BA.4 and BA.2.12.1 are shown in **Table 10.1.** Then the variant (BA.4 and BA.2.12.1) RBD was docked with the ACE2 receptor using HADDOCK docking server [22,23] in order to obtain the S protein (BA.4)-ACE2 and S protein (BA.2.1.1)-ACE2 complex as shown in **Figure 10.1A and 10.1B** respectively.

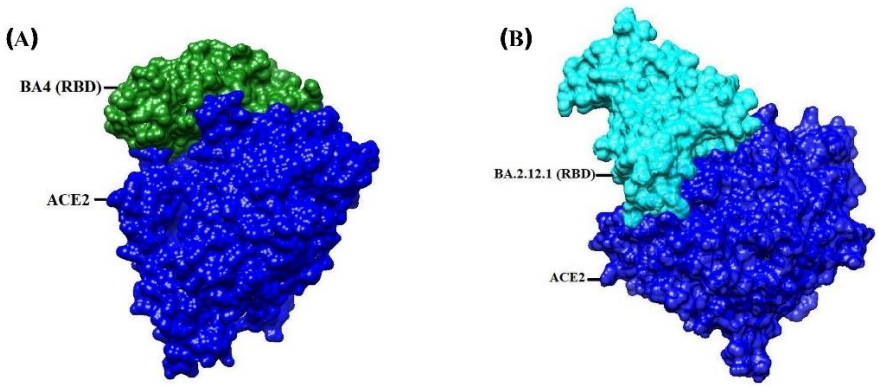

Figure 10.1. *3D structure of* ***(A)*** *SARS-CoV-2 spike receptor-binding domain of BA.4 variant bound with ACE2 (S protein (BA.4)-ACE2)* ***(B)*** *SARS-CoV-2 spike receptor-binding domain of BA.2.12.1 variant bound with ACE2 (S protein (BA.2.12.1)-ACE2).*

Table 10.1. *Mutations (in RBD of Spike Protein) of BA.4 and BA.2.12.1 lineages along with the common muations on both the lineages.*

Mutations of BA.4 lineages	Mutations of BA.2.12.1 lineages	Common mutations of BA.4 and BA.2.12.1 lineages
G339D, S371F, S373P, S375F, T376A, D405N, R408S, K417N, N440K, L452R, S477N, T478K, E484A, F486V, Q498R, N501Y, Y505H	G339D, S371F, S373P, S375F, T376A, D405N, R408S, K417N, N440K, L452Q, S477N, T478K, E484A, Q493R, Q498R, N501Y, Y505H	G339D, S371F, S373P, S375F, T376A, D405N, R408S, K417N, N440K, L452R, S477N, T478K, E484A, Q498R, N501Y, Y505H

10.3.2. Physiochemical parameter analysis

The ExPASY ProtParam [24] online tool was used to analyse the sequences of the BA.2.12.1 and BA.4 variants. Molecular weight, theoretical pI (isoelectric point), amino acid composition, atomic composition, extinction coefficient, estimated half-life, instability index, aliphatic index, and GRAVY (grand average of hydropathicity) are among the computed parameters.

10.3.3. Secondary structure prediction in spike protein of BA.2.12.1 and BA.4 variants

The secondary structure prediction for both BA.2.12.1 and BA.4 variants was done using GOR (Garnier–Osguthorpe–Robson) IV tool [25] which uses information theory and Bayesian statistics to analyze secondary protein structure. The purpose of integrating numerous sequence alignments with GOR is to learn for better secondary structure discrimination.

10.3.4. Identification of conserved residues and mutation

In order to identify the conserved residues and mutations we used Clustal Omega [26] a bioinformatics program, to align the BA.2.12.1 and BA.4 sequences along with the BA.2 sequence. Clustal Omega is a new multiple sequence alignment program that uses seeded guide trees and HMM profile-profile techniques to generate alignments between three or more sequences.

10.3.5. Intrinsically disordered protein prediction

Regions with intrinsic disorder are those that have a dynamic ensemble of conformations but do not develop a stable three-dimensional structure in physiological situations. We used the Predictor of naturally disordered regions (PONDR) (PONDR® VLXT) [27] to determine the disordered regions in both the variants, BA.4 and BA.2.12.1.

10.3.6. Molecular Dynamics Simulations

Both the complex system were then subjected to the process of energy minimization using the steepest descents followed by conjugate gradient minimization technique. Both the complex (S protein (BA.4)-ACE2 complex and S protein (BA.2.12.1)-ACE2 complex) were subjected to MD simulations. The MD simulation was performed using AMBER ff14SB force field with AMBER software package [28,29]. Appropriate number of counter ions were added to the two complex systems to assure their overall neutrality. The two complex systems were solvated with the TIP3P [30] water model and subjected to MD simulations in explicit solvent with solvent buffers of 10Å in all directions. In the first step of minimization, spike receptor-binding domain and ACE2 were fixed with a 500 kcal/mol/Å^2 and the energy of all water molecules and counterions was minimised for 10,000 steepest

descents (SD) steps, followed by 10,000 steps of the conjugate gradient (CG) in the first step of minimization. In order to remove conflicting contacts of the entire complex systems, the second step of minimization was performed in which 12000 steps of SD minimization and 8000 steps of CG minimization were involved. Next, both the complex systems were gradually heated from 0-300K in constant volume (NVT) conditions, thereby applying harmonic restraints with a force constant of 10 kcal/mol/Å^2 on the solute atoms, and equilibration was performed three times with 3000 ps using a force constant of 5.0 kcal/mol/Å. Finally, 100 ns MD simulations were performed using the NPT ensemble without restraints. Particle mesh Ewald [31,32] technique was used to limit the direct space sum to treat the long-range electrostatic interactions with a non-bonded cutoff of 12.0 Å. All the bonds present in the system were constrained using the SHAKE algorithm [33]. The Berendsen weak coupling algorithm [34] was then used to keep a constant pressure and temperature (0.5 ps of heat bath and 0.2 ps of pressure relaxation) throughout the simulation process. The time step of MD simulation was set to 2 fs, and sampling was performed every 10 ps into the MD file.

The lowest energy conformers for both the complex system(S protein (BA.4)-ACE2 and S protein (BA.2.12.1)-ACE2) were extracted using the RMSD clustering algorithm from the highly populated clusters and submitted to the PDBsum server (http://www.ebi.ac.uk/thornton srv/ databases /pdbsum/ Generate. html) for analysing the residue-specific interactions, which are considered to be essential for understanding the nature of interactions. PDBsum [35] is a database that shows schematic diagrams of the non-bonded contacts between amino acid residues at the interface of molecules in a multimer complex.

10.3.7. Binding Free energy calculations

The Molecular Mechanics Generalized Born Surface Area (MM-GBSA) method implemented in AMBER 16 [36,37] package was performed to calculate the binding free energy as well as the free energy decomposition of the two complex systems (S protein (BA.4)-ACE2 and S protein (BA.2.12.1)-ACE2). To determine the relevant energies, 200 snapshots from the last 10 ns of MD trajectories for each complex system were selected.

The formulas for calculating the BFE and their decomposed energetic components are same as described in section 7A.3.2. of Chapter 7A. The approaches and protocols that we have considered in

this study to estimate the binding free energy have been used in many of the recent in-silico studies [38-41] and a similar protocol was employed in our earlier studies on SARS-CoV-2 variants [42-45].

10.4. Results and Discussion:

10.4.1. Physiochemical properties evaluated using ExPASY ProtParam

It includes the total number of amino acid composition, molecular weight, Theoretical pI, estimated half-life, Aliphatic index, Instability index, Grand Hydropathicity Index summarized in **Table 10.2**. With a total of 195 amino acid in both the variant, the molecular weights of the variants BA.4 and BA.2.12.1 are calculated to be 21985.86 and 22033.90 respectively. Theoretical pI is the isoelectric point of a protein where the net negative and positive charge cancels each other. The protein is said to be alkaline if its pI value is greater than 7, and acidic if it is lower than 7.

We observed that both the current variants BA.2.12.1 and BA.4, all are alkaline in nature with a pI of 8.73. Estimated half-life seems to be same in both the variants as 7.2hr. Aliphatic index indicates relative volume occupied by positive amino acids such as alanine, valine, isoleucine, etc. and is found to be 70.46 and 68.97 for BA.4 and BA.2.12.1 respectively. More is the positive score greater is the hydrophobicity indicating stable transmembrane alpha-helices of membrane proteins. Instability index is a measure of stability of proteins. Index less than 40 is considered to be stable while more than 40 is considered to be unstable. It was found to be 25.09 for BA.2.12.1 and 24.90 for BA.4. A protein with a low grand average of hydropathicity (GRAVY) value is nonpolar and has a stronger affinity for water, indicating that it is intrinsically hydrophilic. The GRAVY value was found to be -0.224 for BA.2.12.1 and -0.217 for BA.4 variant

Table 10.2. ExPASY ProtParam data of BA.2.12.1 and BA 4 variant.

Parameters	BA.2.12.1 variant	BA4 variant
Molecular weight (Da)	22033.90	21985.86
Theoretical pI	8.73	8.73
Estimated half-life (mammalian reticulocytes) (Hours)	7.2hr	7.2hr
Aliphatic index	68.97	70.46
Instability index	25.09	24.90
GRAVY (Grand Hydropathicity Index)	-0.224	-0.217

Total no. of negative charges (Asp+Glu)	14	14
Total no. of positive charges (Arg+Lys)	19	19

10.4.2. Prediction of secondary structural changes in spike protein

GOR IV was used to predict the changes in the secondary structure of the spike protein of the RBD region. BA.2.12.1 has a higher alpha helix and extended strand structure, while BA.4 has a higher percentage of random coil, as shown in **Table 10.3**. The predicted increase in alpha helix explains increase in stability of secondary structure (due to formation of hydrogen bonds between an amide hydrogen of one amino acid and a carbonyl oxygen four amino acids away) of the RBD region of BA.2.12.1 while beta strand can extend as much as 35 Â in length which explains the decrease in stability of structure as extension in strands results in increase in distance thereby decreasing the strength of hydrogen bonds. The presence of higher percentage to random coils concludes higher degree of randomness i.e., high entropy due to non-formation of bonds in BA.4 thereby decreasing stability of structure than BA.2.12.1.

Table 10.3. *Structural changes in the RBD region of BA.2.12.1 and BA.4 predicted using GOR IV*

Secondary structure	BA.2.12.1 (%)	BA.4 (%)
Alpha helix (Hh)	6.67%	6.15%
3_{10} helixes (Gg)	0.00%	0.00%
Pi helix (Ii)	0.00%	0.00%
Beta bridge (Bb)	0.00%	0.00%
Extended strand (Ee)	25.64%	20.51%
Beta turn (Tt)	0.00%	0.00%
Bend region (Ss)	0.00%	0.00%
Random coil (Cc)	67.69%	73.33%
Ambiguous stress (?)	0.00%	0.00%
Other states	0.00%	0.00%

The schematic representation of helix, sheet and coil regions of secondary structure for the BA.2.12.1 and BA.4 variant is depicted in **Figure 10.2 and 10.3** respectively.

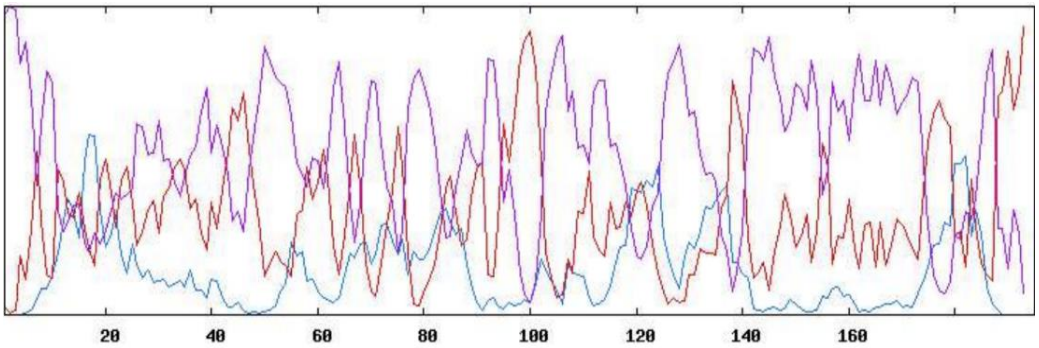

Figure 10.2. *Representation of helix, sheet and coil regions of secondary structure of BA.2.12.1 variant predicted from GOR IV.*

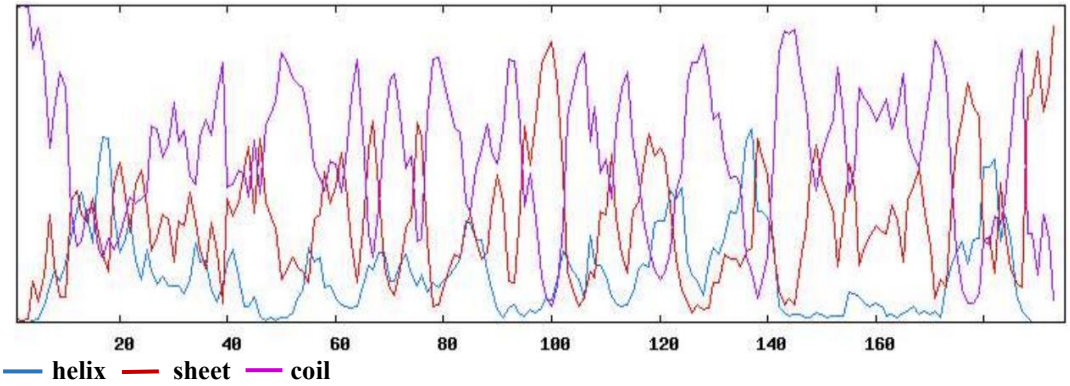

Figure 10.3. *Representation of helix, sheet and coil regions of secondary structure of BA.4 variant predicted from GOR IV.*

10.4.3. Identification of conserved residues and mutation

Clustal Omega was used to align the receptor binding region sequence of the two variants- BA.2.12.1 and BA.4 with respect to BA.2. Analysis depicts the aligned sequence (depicted with *) and the unaligned region (depicted with :) as shown in supplementary **Figure 10.4.** And the unaligned residue was found at residue number 120, 161 and 154.

```
BA2.pdb          TNLCPFDEVFNATRFASVYAWNRKRISNCVADYSVLYNFAPFFAFKCYGVSPTKLNDLCF 60
BA2.12.1.pdb     TNLCPFDEVFNATRFASVYAWNRKRISNCVADYSVLYNFAPFFAFKCYGVSPTKLNDLCF 60
BA4.pdb          TNLCPFDEVFNATRFASVYAWNRKRISNCVADYSVLYNFAPFFAFKCYGVSPTKLNDLCF 60
                 ************************************************************

BA2.pdb          TNVYADSFVIRGNEVSQIAPGQTGNIADYNYKLPDDFTGCVIAWNSNKLDSKVGGNYNYL 120
BA2.12.1.pdb     TNVYADSFVIRGNEVSQIAPGQTGNIADYNYKLPDDFTGCVIAWNSNKLDSKVGGNYNYQ 120
BA4.pdb          TNVYADSFVIRGNEVSQIAPGQTGNIADYNYKLPDDFTGCVIAWNSNKLDSKVGGNYNYR 120
                 ************************************************************:

BA2.pdb          YRLFRKSNLKPFERDISTEIYQAGNKPCNGVAGFNCYFPLRSYGFRPTYGVGHQPYRVVV 180
BA2.12.1.pdb     YRLFRKSNLKPFERDISTEIYQAGNKPCNGVAGFNCYFPLRSYGFRPTYGVGHQPYRVVV 180
BA4.pdb          YRLFRKSNLKPFERDISTEIYQAGNKPCNGVAGVNCYFPLQSYGFRPTYGVGHQPYRVVV 180
                 ********************************:******:********************

BA2.pdb          LSFELLHAPATVCGP   195
BA2.12.1.pdb     LSFELLHAPATVCGP   195
BA4.pdb          LSFELLHAPATVCGP   195
                 ***************
```

Figure 10.4. *Clustal Omega was used to align the receptor binding region sequence ranging from 333-527 of the two variants- BA.2.12.1 and BA.4 with respect to BA.2.*

10.4.4. Intrinsically disordered protein prediction

Intrinsically disordered proteins (IDPs) are unstable, dynamic proteins characterized by tertiary structure abundant in charged and hydrophilic amino acids like Arginine, Proline, Glycine and Serine. IDPs, due to its dynamic state, it continuously changes its structure whilst binding in different sites with different sites. Thus, higher is the disordered residues lower is the binding affinity with the receptor hence decreasing its stability. Here, calculated via PONDR, results verify that the RBD of BA.4 variant possess higher number of disordered region when compared with BA.2.12.1. While same number of disordered regions were found when the entire sequence for spike was considered for the analysis as shown in **Table 10.4**.

Table 10.4. *Intrinsically disordered prediction using PONDR® VLXT*

VARIANT	NO. OF RESIDUES DISORDERED	OVERALL % DISORDERED	PREDICTED DISORDER SEGMENT	NO. OF DISORDERED SEGMENT
BA2.12.1	70	6	[16]-[22] [40]-[40] [601]-[610] [678]-[709] [869]-[871] [982]-[986] [992]-[994] [1023]- [1023] [1160]- [1166]	32
BA2.12.1(RBD)	2	1.03	[77]-[78]	2

BA4	85	6.68	[16]-[22] [40]-[40] [601]-[610] [678]-[709] [869]-[871] [982]-[986] [992]-[994] [1023]- [1023] [1174]- [1194] [1264]- [1264]	32
BA4 (RBD)	29	29	[72]-[81] [117]-[124] [131]-[138] [163]-[165]	4

* **Abbreviation: RBD, receptor-binding domain**

10.4.5. MD simulation of the BA.4 and B.A.2.12.1 variant of SARS-CoV-2 spike receptor-binding domain bound with ACE2.

To study the dynamic properties of the two complexes (S protein (BA.4)-ACE2) and (S protein (BA.2.12.1)-ACE2) MD simulation was carried out for 100 ns. The conformational snapshots of the (S protein (BA.4)-ACE2) and (S protein (BA.2.12.1)-ACE2) complexes during the course of 100 ns MD simulation time at a discrete time interval of 10 ns were depicted in **Figure 10.5** and **Figure 10.6**.

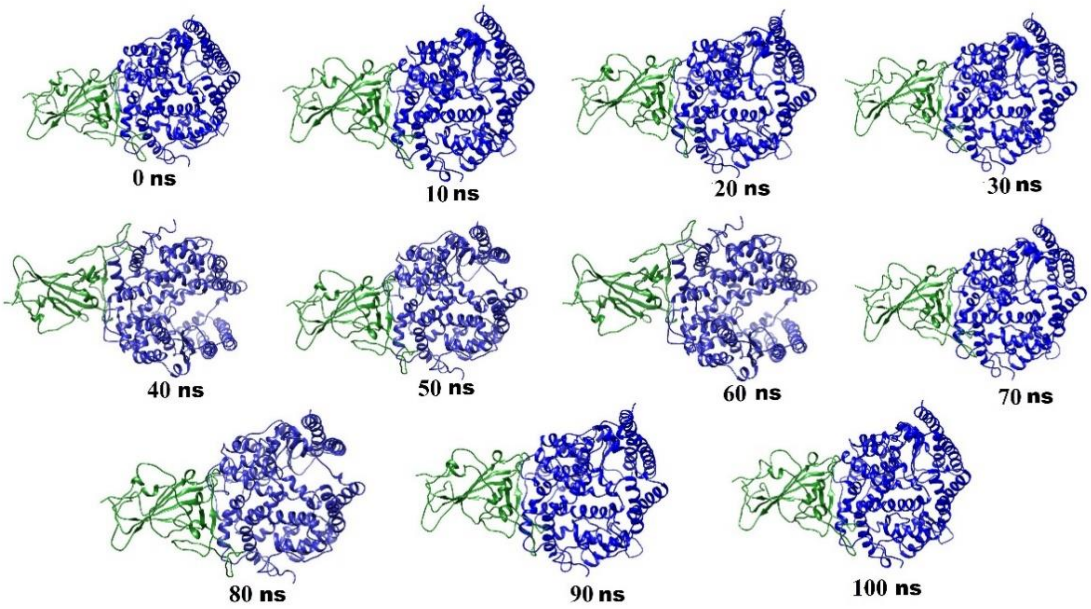

Figure 10.5. *Conformational snapshots of S protein (BA.4)-ACE2 complex at the discrete time interval of 10 ns during the course of 100 ns of MD simulation.*

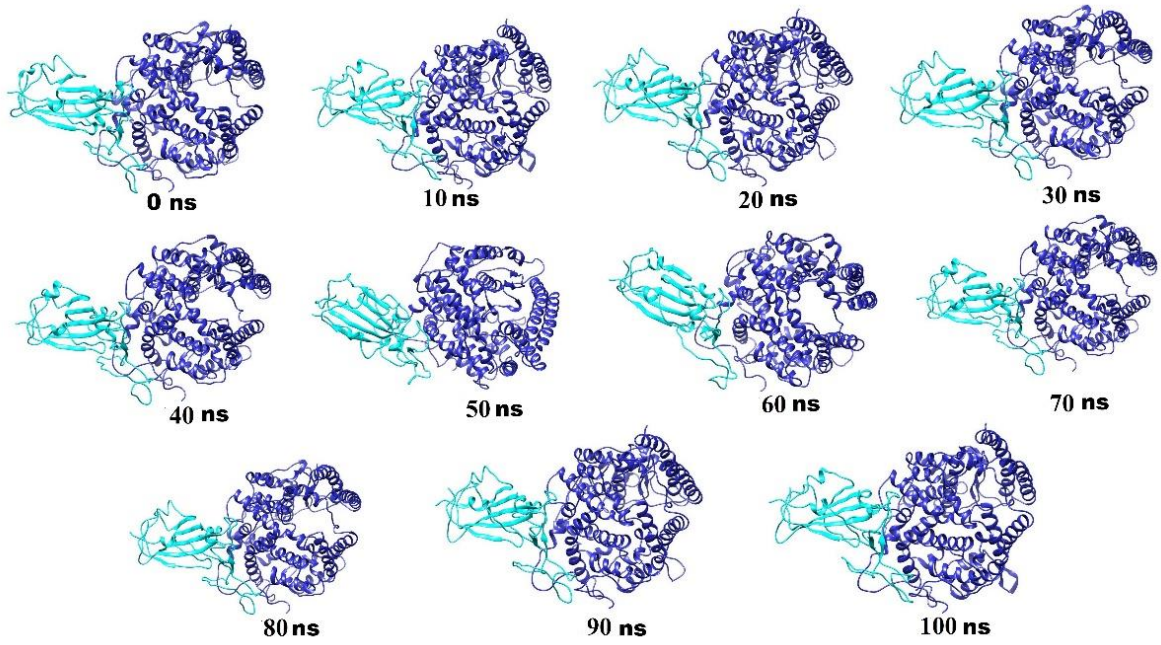

Figure 10.6. *Conformational snapshots of S protein (BA.2.12.1)-ACE2 complex at the discrete time interval of 10 ns during the course of 100 ns of MD simulation.*

10.4.5.1. RMSD Analysis.

The average deviations in the atomic positions and the stability through the trajectory of 100 ns of the MD simulations, the RMSD (root mean square deviation) values of the backbone atoms of the complexes along with the S protein (Apo form) for both BA.4 and BA.2.12.1 were calculated and depicted in **Figure 10.7 and 10.8**. The RMSD of BA.4 type as well as the BA.2.12.1 complex appeared to be stable after 10 ns, revealing that good convergence was achieved for each system. Interestingly, we noticed that the RMSD values of the BA.2.12.1 complex were slightly higher than that of the BA.4 type complex. The average RMSD value of S protein (BA.4) in Apo form was found to be 1.55 Å whereas the RMSD of S protein (BA.4) in complex form was seen to be 1.39 Å which indicated higher stability of the Spike when bound to the ACE2 receptor. A similar pattern was observed in case of BA.2.12.1 variant. The average RMSD value of S protein (BA.2.12.1) in Apo form was found to be 2.03 Å whereas the RMSD of S protein (BA.4) in complex form was seen to be 1.44 Å. We also noticed that the binding of ACE2 reduced the perturbation of S protein to a significant extent in both the complex systems.

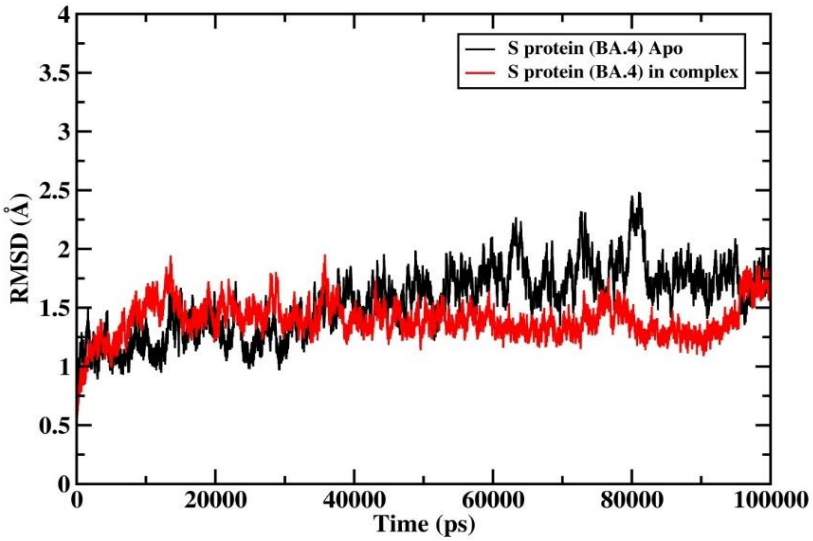

Figure 10.7. *Backbone RMSD's for S protein (BA.4) Apo (black) and S protein (BA.4) in S protein (BA.4)-ACE2 complex (Red)*

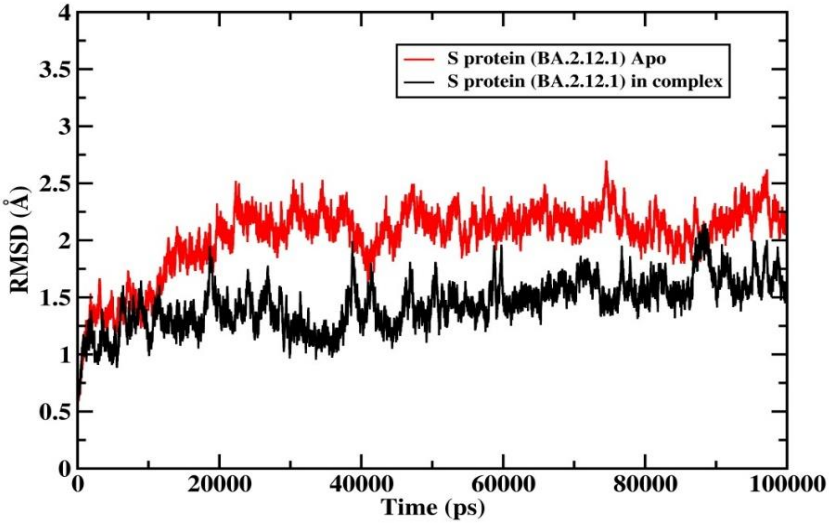

Figure 10.8*. Backbone RMSD's for S protein (BA.2.12.1) Apo (Red) and S protein (BA.2.12.1) in S protein (BA.2.12.1)-ACE2 complex (Black)*

10.4.5.2. RMSF Analysis

We further explored the S protein flexibility in S protein (BA.4)-ACE2) and (S protein (BA.2.12.1)-ACE2) complexes by determining the Cα RMSF values from the MD simulations trajectory analysis. In **Figure 10.9** the RMSF analysis of spike protein (BA.4 and BA.2.12.1) exclusively in the complex has been depicted while in **Figure 10.10** the RMSF analysis for the entire complex has been shown. We observed significant differences in the flexibility of S protein in BA.4, BA.2.12.1 complexes in

particular at the regions in and around the mutation sites mentioned in the Table 10.1. The RMSF values of Cα atoms of S protein in BA.2.12.1 complex shows relatively lower values than in the BA.4 complex. From **Figure 10.9**, it is more apparent that there is significant reduction in structural fluctuations and increased stability in the case of BA.4 and BA.2.12.1 complexes. Among BA.4 and BA.2.12.1 complexes we found the fluctuations are relatively less in the case of BA.2.12.1 complex.

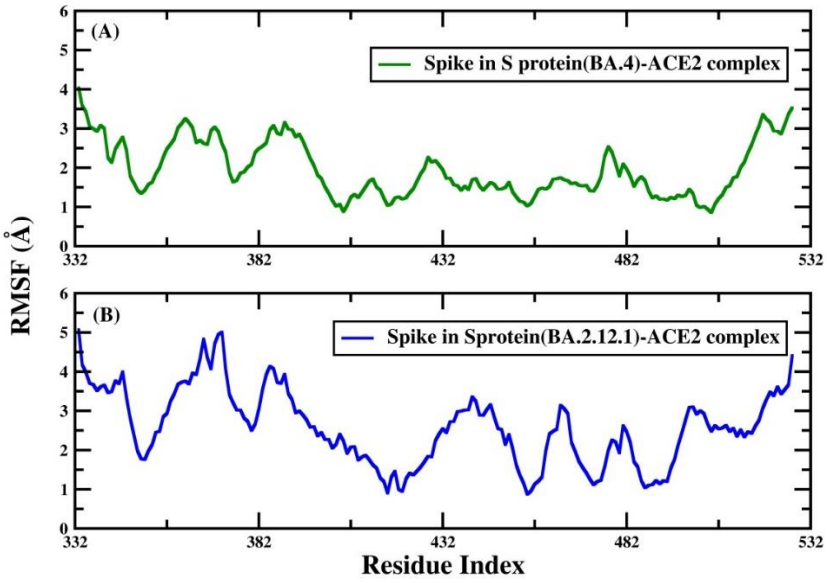

Figure 10.9. *Backbone RMSF's for Spike protein in* ***(A)*** *S protein (BA.4)-ACE2 complex (Green) and* ***(B)*** *S protein (BA.2.12.1)-ACE2 complex (Blue).*

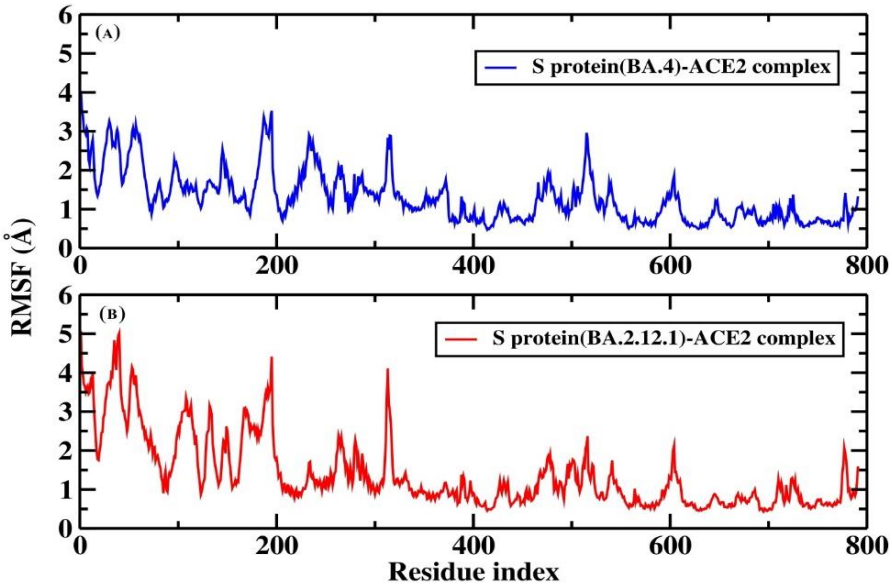

Figure 10.10. *Backbone RMSF's for* ***(A)*** *S protein (BA.4)-ACE2 complex (blue) and* ***(B)*** *S protein (BA.2.12.1)-ACE2 complex (red).*

10.4.5.3. Hydrogen bond Analysis

Additionally, we also calculated and plotted the number of intermolecular hydrogen bonds present in the (S protein (BA.4)-ACE2) and (S protein (BA.2.12.1)-ACE2) complexes as shown in **Figure 10.11** as these hydrogen bonds play a crucial role in conferring the stability to the protein complexes. The number of inter-molecular hydrogen bonds was found to be significantly higher in S protein (BA.2.12.1)-ACE2 complex as compared to the S protein (BA.4)-ACE2 complex.

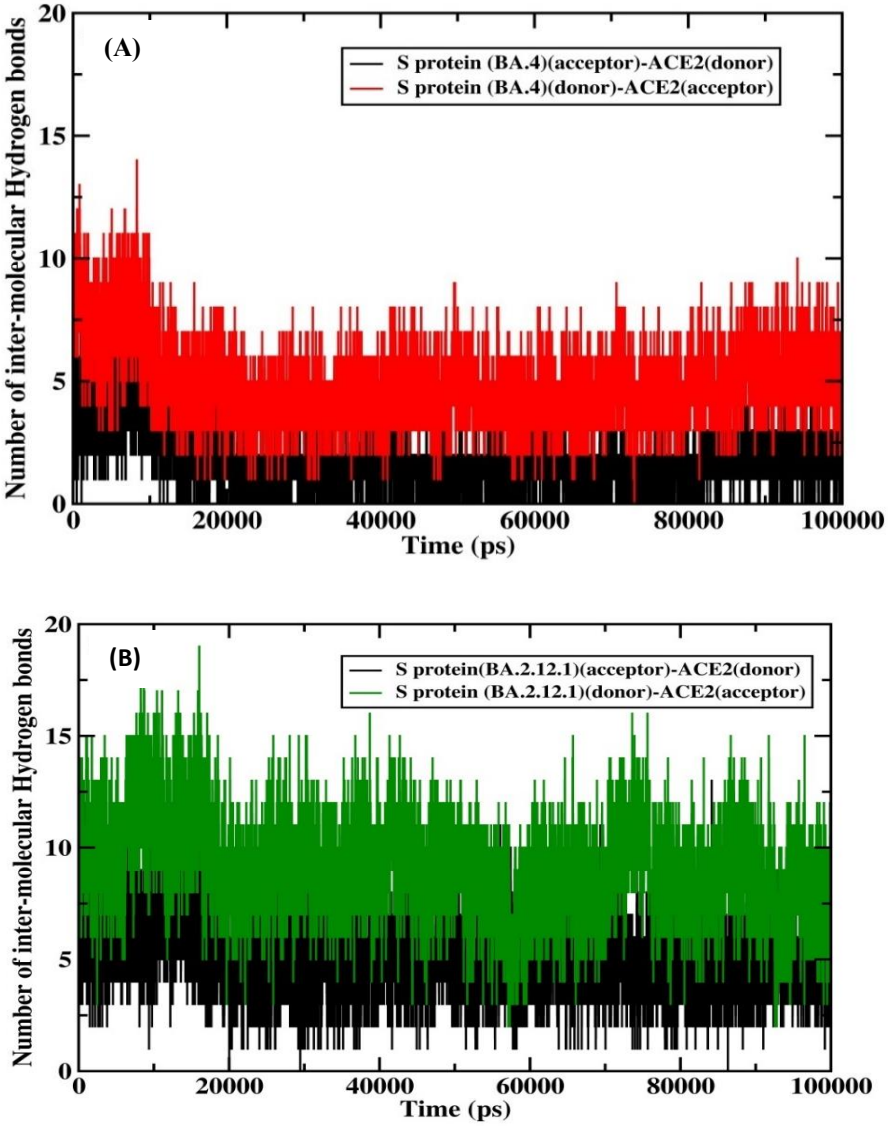

Figure 10.11. *Number of intermolecular hydrogen bonds between S protein and ACE2 in* ***(A)*** *S protein (BA.4)-ACE2 complex* ***(B)*** *S protein (BA.2.12.1)-ACE2 complex.*

The list of intermolecular hydrogen bonds noticed between the S protein (acceptor/donor) and ACE2 (donor/acceptor) during the last 20 ns of MD simulation of both the complexes were summarized in **Table 10.5-10.8.**

Table 10.5: *Hydrogen bond analysis of S protein (BA.4)-ACE2 complex during the last 20 ns of MD simulation with S protein as acceptor and ACE2 as donor.*

Acceptor	DonorH	Donor	Frac	Average Distance(Å)	Average Angles (º)
ASN_108@O	ALA_334@H	ALA_334@N	0.2848	2.8614	154.9717
GLU_8@OE1	ARG_308@HH21	ARG_308@NH2	0.1338	2.8085	152.6348
GLU_8@OE1	ARG_308@HE	ARG_308@NE	0.1322	2.8337	156.2533
GLU_8@OE2	ARG_308@HH21	ARG_308@NH2	0.1237	2.8006	153.867
ASN_22@OD1	GLN_469@HE21	GLN_469@NE2	0.1182	2.8541	160.1179
ASN_2@OD1	LYS_388@HZ2	LYS_388@NZ	0.095	2.814	155.247
ASN_28@OD1	LYS_388@HZ3	LYS_388@NZ	0.092	2.8148	155.7004
ASN_28@OD1	LYS_388@HZ2	LYS_388@NZ	0.0853	2.8167	155.4032
GLU_8@OE2	ARG_308@HE	ARG_308@NE	0.0836	2.8348	155.9654
ASN_2@OD1	LYS_388@HZ1	LYS_388@NZ	0.0815	2.8058	155.5292
ARG_23@O	ARG_467@HE	ARG_467@NE	0.08	2.8295	151.1265
ASN_22@OD1	ARG_467@HH21	ARG_467@NH2	0.0784	2.842	153.0776
ASN_22@OD1	ARG_467@HE	ARG_467@NE	0.0774	2.8655	154.9174
ASN_2@OD1	LYS_388@HZ3	LYS_388@NZ	0.0733	2.8128	156.2279
SER_41@OG	LYS_319@HZ1	LYS_319@NZ	0.071	2.8584	153.968
SER_41@OG	LYS_319@HZ2	LYS_319@NZ	0.0708	2.8574	154.1554
ASN_28@OD1	LYS_388@HZ1	LYS_388@NZ	0.068	2.8222	155.5825
ASN_22@OD1	GLN_469@HE22	GLN_469@NE2	0.062	2.8552	161.4501
SER_41@OG	LYS_319@HZ3	LYS_319@NZ	0.0611	2.8541	153.5588
ARG_25@O	GLN_469@HE21	GLN_469@NE2	0.045	2.8768	161.9907
ARG_25@O	ARG_467@HH11	ARG_467@NH1	0.0406	2.828	153.0566
SER_27@O	LYS_390@HZ1	LYS_390@NZ	0.0358	2.8134	153.267
PRO_195@OXT	THR_376@HG1	THR_376@OG1	0.0352	2.7029	163.2477
SER_27@O	LYS_390@HZ3	LYS_390@NZ	0.0266	2.8213	153.8259
SER_27@O	LYS_390@HZ2	LYS_390@NZ	0.0256	2.8167	153.2492
ASN_28@O	LYS_388@HZ3	LYS_388@NZ	0.0256	2.8272	152.0951
ALA_20@O	GLN_469@HE21	GLN_469@NE2	0.0245	2.8729	161.9902
GLU_139@OE2	LYS_474@HZ1	LYS_474@NZ	0.0243	2.8081	159.2613
PRO_195@O	THR_376@HG1	THR_376@OG1	0.024	2.7039	165.2798
TRP_21@O	GLN_469@HE21	GLN_469@NE2	0.0237	2.8866	159.1855
GLU_139@OE2	LYS_474@HZ3	LYS_474@NZ	0.0204	2.8112	159.2395
ASN_28@O	LYS_390@HZ2	LYS_390@NZ	0.0204	2.8415	150.4481
ARG_23@O	ARG_467@HH21	ARG_467@NH2	0.0198	2.8194	145.968
ASN_2@OD1	LYS_390@HZ1	LYS_390@NZ	0.0174	2.8283	151.1424
ASN_28@O	LYS_390@HZ3	LYS_390@NZ	0.017	2.8367	150.6502
SER_39@O	LYS_319@HZ3	LYS_319@NZ	0.0169	2.82	148.3886

SER_39@O	LYS_319@HZ1	LYS_319@NZ	0.0163	2.8148	149.7552
SER_39@O	LYS_319@HZ2	LYS_319@NZ	0.0161	2.82	150.317
ASN_28@O	LYS_390@HZ1	LYS_390@NZ	0.0159	2.8453	149.6366
ASN_11@OD1	THR_307@HG1	THR_307@OG1	0.0156	2.7416	161.6031
ASN_2@OD1	LYS_390@HZ3	LYS_390@NZ	0.0155	2.8212	151.0807
ALA_40@O	LYS_319@HZ2	LYS_319@NZ	0.015	2.8329	156.3451
SER_27@OG	ARG_467@HH21	ARG_467@NH2	0.0138	2.855	155.5724
GLU_139@OE1	LYS_474@HZ1	LYS_474@NZ	0.0136	2.8077	156.6223
ASP_32@OD1	GLN_373@HE22	GLN_373@NE2	0.0134	2.8296	163.6244
ASN_2@OD1	LYS_390@HZ2	LYS_390@NZ	0.013	2.8267	150.9027
THR_1@O	GLN_392@HE22	GLN_392@NE2	0.0111	2.8658	157.111
ASN_28@O	LYS_388@HZ2	LYS_388@NZ	0.011	2.8348	148.557
ASN_28@O	LYS_388@HZ1	LYS_388@NZ	0.0099	2.8463	150.1378
SER_137@HB3	ILE_473@HA	ILE_473@CA	0.009	2.9307	146.2025
ARG_23@O	GLN_469@HE22	GLN_469@NE2	0.0082	2.8542	158.4547
GLU_139@OE2	LYS_474@HZ2	LYS_474@NZ	0.0078	2.8046	158.155
ARG_14@HG2	ASN_552@HA	ASN_552@CA	0.0075	2.9432	146.1692
ASN_2@OD1	LYS_390@H	LYS_390@N	0.0071	2.8806	156.8198
GLY_7@HA3	ALA_312@HA	ALA_312@CA	0.0064	2.9299	141.913
ALA_40@O	LYS_319@HZ3	LYS_319@NZ	0.0062	2.8284	150.4823
SER_41@HG	LYS_319@HZ3	LYS_319@NZ	0.006	2.8668	151.1486
ASN_28@HD21	LYS_388@HG2	LYS_388@CG	0.0057	2.8731	149.1621
ASN_108@HA	LEU_332@HA	LEU_332@CA	0.0057	2.9251	142.4389
ARG_23@O	GLN_469@HE21	GLN_469@NE2	0.0054	2.8469	152.9002
SER_41@HG	LYS_319@HZ1	LYS_319@NZ	0.005	2.8814	147.5267

Table 10.6. *Hydrogen bond analysis of S protein (BA.4)-ACE2 complex during the last 20 ns of MD simulation with S protein as donor and ACE2 as acceptor.*

Acceptor	DonorH	Donor	Frac	Average Distance (Å)	Average Angles (º)
ASP_551@OD1	ARG_14@HH21	ARG_14@NH2	0.5133	2.8003	159.8873
THR_330@O	ASN_108@HD22	ASN_108@ND2	0.4934	2.8511	161.7927
ASP_551@OD2	ARG_14@HE	ARG_14@NE	0.4498	2.841	160.421
ASP_551@OD2	ARG_14@HH21	ARG_14@NH2	0.3548	2.8061	157.2295
ASP_551@OD2	ARG_14@H	ARG_14@N	0.3527	2.854	159.5868
ASP_551@OD2	THR_13@H	THR_13@N	0.263	2.858	154.3543
GLU_315@OE2	ASN_11@HD22	ASN_11@ND2	0.2415	2.8214	163.6516
ASP_551@OD1	ARG_14@HE	ARG_14@NE	0.2245	2.8462	160.8716
ASP_551@OD1	ARG_14@H	ARG_14@N	0.2143	2.8426	157.9829
ARG_331@O	ASN_107@HD22	ASN_107@ND2	0.182	2.8382	160.9025
ASP_551@OD1	THR_13@H	THR_13@N	0.1804	2.8538	156.7026
ALA_468@O	ARG_134@HH11	ARG_134@NH1	0.1742	2.8175	150.8829
GLU_387@O	ASN_28@HD21	ASN_28@ND2	0.1586	2.854	157.3339
VAL_466@O	ARG_25@HH11	ARG_25@NH1	0.1575	2.8117	157.4791

GLU_315@OE2	SER_41@HG	SER_41@OG	0.153	2.6699	162.6543
ALA_380@O	ASN_2@HD22	ASN_2@ND2	0.1452	2.8483	162.2086
GLN_469@OE1	ARG_25@H	ARG_25@N	0.1312	2.8586	161.8669
GLU_465@OE1	SER_27@HG	SER_27@OG	0.1289	2.6691	163.6608
GLN_469@OE1	ARG_23@H	ARG_23@N	0.114	2.8736	160.2489
GLU_315@OE1	SER_41@HG	SER_41@OG	0.1006	2.6836	163.3554
GLU_377@OE1	LYS_54@HZ2	LYS_54@NZ	0.0972	2.7854	159.9101
GLU_377@OE2	LYS_54@HZ3	LYS_54@NZ	0.0789	2.7782	159.6595
GLU_377@O	THR_1@HG1	THR_1@OG1	0.0744	2.7271	163.33
ALA_381@O	ASN_2@H	ASN_2@N	0.0738	2.8679	161.1065
LYS_390@O	THR_1@H2	THR_1@N	0.0728	2.8182	152.3783
LYS_390@O	THR_1@H1	THR_1@N	0.0687	2.8196	152.2007
GLN_464@O	ARG_25@HH11	ARG_25@NH1	0.0596	2.8477	156.673
GLU_377@OE1	LYS_54@HZ1	LYS_54@NZ	0.0545	2.7812	158.0505
LYS_390@O	THR_1@H3	THR_1@N	0.0539	2.8195	151.2948
GLU_465@OE2	SER_27@HG	SER_27@OG	0.0536	2.6935	162.121
GLU_377@OE2	LYS_54@HZ2	LYS_54@NZ	0.0516	2.7939	156.0613
ALA_312@O	ASN_11@HD21	ASN_11@ND2	0.0494	2.8467	158.4731
ASP_549@OD1	LYS_24@HZ3	LYS_24@NZ	0.0491	2.8186	154.7262
GLU_377@OE2	LYS_54@HZ1	LYS_54@NZ	0.0435	2.7819	157.049
ASP_551@OD1	THR_13@HG1	THR_13@OG1	0.0422	2.7106	161.0699
ASP_549@OD2	LYS_24@HZ1	LYS_24@NZ	0.042	2.8214	154.0752
LYS_333@O	ASN_108@HD22	ASN_108@ND2	0.038	2.8701	154.7872
ASP_549@OD1	LYS_24@HZ1	LYS_24@NZ	0.036	2.8207	155.1742
ASP_549@OD2	LYS_24@HZ3	LYS_24@NZ	0.0356	2.8274	152.5154
GLU_387@OE1	ASN_28@HD21	ASN_28@ND2	0.0353	2.8429	160.2944
ASP_549@OD2	LYS_24@HZ2	LYS_24@NZ	0.0347	2.8261	154.0473
GLU_387@OE2	ASN_28@HD21	ASN_28@ND2	0.0306	2.841	159.47
GLU_374@OE2	LYS_54@HZ1	LYS_54@NZ	0.0302	2.79	157.2421
GLU_374@OE1	LYS_54@HZ1	LYS_54@NZ	0.0291	2.7835	156.5435
ASP_551@OD2	THR_13@HG1	THR_13@OG1	0.028	2.7184	159.6033
ASP_549@O	LYS_24@HZ1	LYS_24@NZ	0.0263	2.8342	153.112
GLU_374@OE1	LYS_54@HZ3	LYS_54@NZ	0.0257	2.7808	157.1073
ASP_549@OD1	LYS_24@HZ2	LYS_24@NZ	0.0254	2.8245	154.3738
GLU_374@OE2	LYS_54@HZ2	LYS_54@NZ	0.022	2.7738	157.7041
GLU_374@OE2	LYS_54@HZ3	LYS_54@NZ	0.0214	2.7835	157.3532
GLU_364@OE1	THR_1@H3	THR_1@N	0.0204	2.8073	155.9293
GLU_364@OE1	THR_1@H1	THR_1@N	0.019	2.813	154.2079
LEU_378@O	THR_1@HG1	THR_1@OG1	0.0178	2.773	161.9267
GLU_374@OE1	LYS_54@HZ2	LYS_54@NZ	0.0175	2.7843	156.3019
ASP_549@O	LYS_24@HZ2	LYS_24@NZ	0.0165	2.8339	151.2607
ASP_549@O	LYS_24@HZ3	LYS_24@NZ	0.0163	2.832	151.4358
GLU_315@OE2	ASN_11@HD21	ASN_11@ND2	0.0161	2.8017	163.1959
THR_307@O	ASN_11@HD21	ASN_11@ND2	0.0158	2.8727	157.9253

GLN_392@OE1	THR_1@H1	THR_1@N	0.0158	2.827	149.8726
GLN_392@OE1	THR_1@H3	THR_1@N	0.0158	2.8226	149.8199
GLN_392@OE1	THR_1@H2	THR_1@N	0.0151	2.8312	149.8318
LYS_388@O	ASN_2@HD21	ASN_2@ND2	0.0141	2.8537	153.3506
THR_376@OG1	THR_1@HG1	THR_1@OG1	0.0132	2.813	159.9506
GLU_377@OE1	LYS_54@HZ3	LYS_54@NZ	0.0128	2.7961	155.1329
GLU_364@OE1	THR_1@H2	THR_1@N	0.0114	2.806	157.014
ARG_308@O	ASN_11@HD22	ASN_11@ND2	0.0113	2.8662	150.3261
ASN_552@HA	ARG_14@HG2	ARG_14@CG	0.0106	2.9427	144.2634
LEU_332@O	ASN_107@HD22	ASN_107@ND2	0.01	2.8469	158.5659
THR_330@OG1	ASN_108@HD22	ASN_108@ND2	0.01	2.9006	164.7733

Table 10.7. *Hydrogen bond analysis of S protein (BA.2.12.1)-ACE2 complex during the last 20 ns of MD simulation with S protein as acceptor and ACE2 as donor.*

Acceptor	**DonorH**	**Donor**	**Frac**	**Average Distance (Å)**	**Average Angles (º)**
VAL_75@O	SER_441@H	SER_441@N	0.7047	2.8555	160.1122
ASP_73@OD1	ARG_322@HH22	ARG_322@NH2	0.7035	2.7892	161.6997
ASP_73@OD2	ARG_322@HH11	ARG_322@NH1	0.6994	2.8093	163.5115
PRO_167@O	GLN_670@HE21	GLN_670@NE2	0.5853	2.845	162.4634
ARG_76@O	SER_449@HG	SER_449@OG	0.554	2.7448	161.7508
GLN_174@OE1	ALA_659@H	ALA_659@N	0.5418	2.8713	160.5658
GLU_74@O	ASP_444@H	ASP_444@N	0.5283	2.8407	151.0588
GLU_74@O	GLU_443@H	GLU_443@N	0.4858	2.8759	152.9664
GLY_115@O	ASN_696@H	ASN_696@N	0.3154	2.8602	159.6656
GLN_174@OE1	ILE_658@H	ILE_658@N	0.2989	2.8604	150.8622
GLN_77@O	ALA_446@H	ALA_446@N	0.2406	2.893	160.2217
ASN_169@OD1	LEU_662@H	LEU_662@N	0.1466	2.9156	160.1472
ASP_95@OD2	ARG_447@HH11	ARG_447@NH1	0.1412	2.792	154.7283
ASP_73@OD2	ARG_322@HH22	ARG_322@NH2	0.1384	2.8125	156.3612
THR_168@OG1	GLY_660@H	GLY_660@N	0.1254	2.9125	156.8478
GLN_82@OE1	GLN_450@HE21	GLN_450@NE2	0.1132	2.8517	161.5789
GLN_166@OE1	GLN_670@HE22	GLN_670@NE2	0.106	2.8639	162.5295
GLN_77@O	ARG_447@H	ARG_447@N	0.1001	2.8466	146.8759
ASP_95@OD1	ARG_447@HH11	ARG_447@NH1	0.0941	2.8013	154.1576
VAL_171@O	ARG_322@HH12	ARG_322@NH1	0.0936	2.811	152.712
ASP_95@OD2	ARG_447@HH22	ARG_447@NH2	0.0855	2.824	150.3213
GLN_77@O	GLN_450@HE21	GLN_450@NE2	0.0766	2.8289	157.8841
ASP_95@OD1	ARG_447@HH22	ARG_447@NH2	0.0751	2.8222	151.4778
ASN_116@OD1	ASN_696@HD22	ASN_696@ND2	0.0708	2.8708	161.5225
THR_83@O	GLN_450@HE22	GLN_450@NE2	0.0646	2.8708	159.1468
GLN_77@OE1	SER_449@HG	SER_449@OG	0.0532	2.724	159.9681
ASN_149@O	HIE_713@HE2	HIE_713@NE2	0.0523	2.8452	157.6379

ARG_76@HD2	VAL_442@HA	VAL_442@CA	0.0493	2.9343	148.3705
GLN_166@O	GLY_660@H	GLY_660@N	0.049	2.8668	161.5909
ASN_116@OD1	ASN_696@HD21	ASN_696@ND2	0.0458	2.847	161.0551
GLN_77@O	GLN_450@HE22	GLN_450@NE2	0.0444	2.8343	153.5234
ILE_78@O	ALA_445@H	ALA_445@N	0.0428	2.8357	145.1541
VAL_113@O	LYS_694@HZ1	LYS_694@NZ	0.0418	2.8156	149.4991
VAL_113@O	LYS_694@HZ3	LYS_694@NZ	0.0394	2.8147	151.7217
SER_111@O	LYS_694@HZ3	LYS_694@NZ	0.0382	2.8303	151.9852
VAL_113@O	LYS_694@HZ2	LYS_694@NZ	0.0372	2.8192	150.017
SER_111@O	LYS_694@HZ1	LYS_694@NZ	0.0358	2.8379	152.3057
SER_111@O	LYS_694@HZ2	LYS_694@NZ	0.0308	2.8368	152.2202
GLU_74@H	SER_441@HB3	SER_441@CB	0.03	2.8833	145.5468
THR_168@H	ALA_659@HA	ALA_659@CA	0.0286	2.9008	153.4567
GLN_174@HE21	GLU_656@HA	GLU_656@CA	0.0272	2.9085	146.3871
GLN_161@OE1	LYS_663@HZ2	LYS_663@NZ	0.0263	2.8187	153.5414
ASP_110@O	LYS_694@HZ1	LYS_694@NZ	0.0261	2.8261	152.1725
ASN_169@OD1	HIE_661@H	HIE_661@N	0.0246	2.8644	151.2584
ASN_116@O	LYS_694@HZ2	LYS_694@NZ	0.0246	2.8298	157.997
GLY_115@O	LYS_694@HZ2	LYS_694@NZ	0.0232	2.8179	154.3661
ASN_169@HD21	HIE_661@H	HIE_661@N	0.0224	2.8979	146.213
GLN_82@OE1	GLN_450@HE22	GLN_450@NE2	0.0217	2.8732	157.7109
GLN_161@OE1	LYS_663@HZ3	LYS_663@NZ	0.0216	2.8232	152.2353
THR_83@OG1	GLN_450@HE22	GLN_450@NE2	0.0211	2.8696	154.4757
GLU_74@H	SER_441@HB2	SER_441@CB	0.0208	2.8321	146.6557
GLN_161@OE1	LYS_663@HZ1	LYS_663@NZ	0.0199	2.8161	153.4922
TYR_163@O	TYR_695@HH	TYR_695@OH	0.0198	2.7752	156.1283
ASP_110@O	LYS_694@HZ2	LYS_694@NZ	0.0192	2.8242	151.0537
ASP_110@O	LYS_694@HZ3	LYS_694@NZ	0.0185	2.8185	152.5714
GLY_115@O	LYS_694@HZ3	LYS_694@NZ	0.0173	2.8178	154.4665
TYR_173@HB3	GLY_660@HA2	GLY_660@CA	0.0171	2.9391	142.9172
ASN_116@O	LYS_694@HZ1	LYS_694@NZ	0.0168	2.828	157.2326
GLY_172@O	ARG_322@HH11	ARG_322@NH1	0.0166	2.8205	146.4888
GLN_166@OE1	TYR_695@HH	TYR_695@OH	0.0161	2.7512	159.7219
GLU_74@HB3	SER_441@HB2	SER_441@CB	0.0152	2.9202	140.9111
PRO_80@O	ARG_447@HH22	ARG_447@NH2	0.0149	2.8414	149.6966
ASN_116@O	LYS_694@HZ3	LYS_694@NZ	0.0144	2.8275	158.6773
TYR_173@HB2	GLY_660@HA2	GLY_660@CA	0.0144	2.9413	141.6586
GLY_114@O	ASN_696@HD22	ASN_696@ND2	0.0138	2.8462	156.6316
GLY_115@O	LYS_694@HZ1	LYS_694@NZ	0.0136	2.8196	152.5946
SER_43@O	ARG_653@HH21	ARG_653@NH2	0.0124	2.8519	151.3182
SER_43@OG	LYS_652@HZ1	LYS_652@NZ	0.0116	2.8702	149.7739
PRO_167@HD3	LEU_691@HB3	LEU_691@CB	0.0113	2.9349	142.9347
ALA_40@O	LYS_652@HZ3	LYS_652@NZ	0.011	2.8153	151.0345
ASN_169@H	GLY_660@HA3	GLY_660@CA	0.011	2.8581	149.7505

Table 10.8. *Hydrogen bond analysis of S protein (BA.2.12.1)-ACE2 complex during the last 20 ns of MD simulation with S protein as donor and ACE2 as acceptor.*

#Acceptor	DonorH	Donor	Frac	Average Distance (Å)	Average Angles (°)
ASP_444@O	ARG_76@H	ARG_76@N	0.9486	2.8111	164.6075
LEU_662@O	THR_168@HG1	THR_168@OG1	0.7456	2.7476	162.9437
GLU_656@OE2	ASN_107@HD22	ASN_107@ND2	0.6328	2.8281	164.8966
GLU_443@OE1	ARG_71@HH22	ARG_71@NH2	0.5279	2.7773	158.4681
GLU_443@O	GLN_77@H	GLN_77@N	0.4509	2.8784	151.9572
ASN_657@O	VAL_171@H	VAL_171@N	0.4257	2.8769	160.8309
ASN_657@OD1	GLY_172@H	GLY_172@N	0.3812	2.8824	159.2124
GLU_443@O	ILE_78@H	ILE_78@N	0.3805	2.8534	153.869
GLU_656@OE1	ASN_105@HD22	ASN_105@ND2	0.3597	2.8459	161.8646
ASP_319@OD2	ARG_76@HH12	ARG_76@NH1	0.3402	2.7967	153.1788
ASP_319@OD1	ARG_76@HH11	ARG_76@NH1	0.2814	2.7991	159.2412
ASP_319@OD2	ARG_76@HH22	ARG_76@NH2	0.2684	2.8098	149.8818
GLU_443@OE2	ARG_71@HH22	ARG_71@NH2	0.237	2.7766	159.3117
ASP_693@O	GLN_166@HE22	GLN_166@NE2	0.2046	2.85	161.552
GLU_656@OE2	GLN_174@HE22	GLN_174@NE2	0.1957	2.7977	150.4254
ASP_444@OD2	LYS_46@HZ1	LYS_46@NZ	0.1766	2.7718	156.6219
GLU_656@OE1	ASN_105@HD21	ASN_105@ND2	0.1554	2.8384	163.2509
ASP_444@OD2	LYS_46@HZ2	LYS_46@NZ	0.1496	2.7715	157.1805
HIE_661@ND1	ASN_169@HD21	ASN_169@ND2	0.1416	2.917	152.9534
ASP_444@OD2	LYS_46@HZ3	LYS_46@NZ	0.1344	2.7708	156.9466
ILE_658@O	THR_168@H	THR_168@N	0.1256	2.9028	157.8484
ASP_693@OD2	GLY_115@H	GLY_115@N	0.1202	2.8683	158.4398
GLN_450@OE1	GLN_77@HE22	GLN_77@NE2	0.1191	2.8366	158.18
ASP_444@OD1	LYS_46@HZ1	LYS_46@NZ	0.1185	2.7723	156.8832
SER_441@O	GLU_74@H	GLU_74@N	0.0957	2.9153	159.6169
ASP_444@OD1	LYS_46@HZ3	LYS_46@NZ	0.0914	2.773	158.7997
GLU_443@OE1	ARG_71@HH12	ARG_71@NH1	0.0892	2.8479	148.3398
HIE_687@ND1	ASN_108@HD22	ASN_108@ND2	0.0812	2.9122	160.093
GLN_450@OE1	GLN_82@HE22	GLN_82@NE2	0.0724	2.8423	159.8648
ASP_444@O	GLN_77@H	GLN_77@N	0.0688	2.802	141.8012
ASP_319@OD2	ARG_76@HH11	ARG_76@NH1	0.0648	2.7982	156.7966
ASP_444@OD1	LYS_46@HZ2	LYS_46@NZ	0.0636	2.7799	156.3437
ARG_447@O	GLN_82@HE21	GLN_82@NE2	0.0573	2.8827	156.3259
LYS_694@O	GLN_166@HE22	GLN_166@NE2	0.0561	2.8528	151.7299
ALA_659@HA	THR_168@H	THR_168@N	0.0518	2.8779	149.9434
GLN_450@OE1	THR_83@HG1	THR_83@OG1	0.0515	2.7683	160.5969
TYR_695@OH	SER_162@HG	SER_162@OG	0.0513	2.8218	160.037
VAL_442@HA	ARG_76@HD2	ARG_76@CD	0.051	2.9208	142.8311
GLN_450@OE1	THR_83@H	THR_83@N	0.0472	2.8485	160.4471

ASP_693@OD1	GLY_115@H	GLY_115@N	0.0459	2.8846	158.5326
CYS_655@O	GLN_174@HE21	GLN_174@NE2	0.0424	2.8983	154.3182
GLU_649@OE1	SER_43@HG	SER_43@OG	0.04	2.7099	163.1139
ASN_657@O	GLY_172@H	GLY_172@N	0.0389	2.8959	154.2287
HIE_687@O	ASN_108@HD21	ASN_108@ND2	0.0363	2.8636	152.6256
SER_441@HB3	GLU_74@H	GLU_74@N	0.0362	2.8584	143.7025
SER_449@O	GLN_77@HE22	GLN_77@NE2	0.0357	2.8697	159.5434
GLU_656@OE1	ASN_107@HD22	ASN_107@ND2	0.0305	2.8415	164.3923
GLU_649@OE2	SER_43@HG	SER_43@OG	0.0287	2.6952	164.0282
GLN_450@OE1	GLN_82@HE21	GLN_82@NE2	0.0287	2.842	159.9156
GLU_656@OE2	ASN_105@HD22	ASN_105@ND2	0.0284	2.8511	160.4425
HIE_661@H	ASN_169@HD21	ASN_169@ND2	0.0276	2.8945	144.6222
SER_449@OG	ARG_76@HH21	ARG_76@NH2	0.0264	2.879	156.9624
SER_686@O	ASN_108@HD21	ASN_108@ND2	0.0264	2.859	150.5495
ASP_319@OD1	ARG_76@HE	ARG_76@NE	0.025	2.8722	149.8167
LYS_663@O	GLN_166@HE22	GLN_166@NE2	0.0228	2.8465	156.343
ASP_444@HB3	GLU_74@HA	GLU_74@CA	0.0226	2.933	140.9535
LYS_663@O	GLN_166@HE21	GLN_166@NE2	0.0216	2.8587	152.3819
GLU_698@OE2	ASN_116@HD22	ASN_116@ND2	0.0214	2.8206	161.7276
PHE_395@HE2	VAL_171@H	VAL_171@N	0.0203	2.8088	146.2483
GLU_656@OE2	ASN_105@HD21	ASN_105@ND2	0.0202	2.8515	156.9697
SER_441@HB2	GLU_74@HB3	GLU_74@CB	0.0192	2.9165	140.4043
GLU_698@OE1	ASN_116@HD22	ASN_116@ND2	0.0189	2.8218	162.5682
SER_449@O	GLN_77@HE21	GLN_77@NE2	0.0169	2.883	159.6835
GLY_660@HA3	ASN_169@H	ASN_169@N	0.0165	2.84	151.4003
LYS_372@O	ASN_169@HD22	ASN_169@ND2	0.016	2.8654	160.0378
ALA_690@O	LYS_112@HZ3	LYS_112@NZ	0.0156	2.8182	154.2844
LEU_691@HB3	PRO_167@HD3	PRO_167@CD	0.0154	2.9432	145.9466
ALA_690@O	SER_111@HG	SER_111@OG	0.0147	2.7396	160.6911
ASP_319@OD2	ARG_76@HE	ARG_76@NE	0.0143	2.8541	151.0787
ARG_447@HA	GLN_82@HE21	GLN_82@NE2	0.0136	2.8175	143.7613
HIE_713@O	ASN_149@HD21	ASN_149@ND2	0.0134	2.8577	158.74
VAL_442@HA	ARG_76@HB2	ARG_76@CB	0.0133	2.9318	140.514
GLU_443@OE2	ARG_71@HH12	ARG_71@NH1	0.0131	2.857	147.5152
ILE_658@HG23	GLN_174@HE21	GLN_174@NE2	0.013	2.8353	143.1683
GLN_450@OE1	GLN_77@HE21	GLN_77@NE2	0.012	2.8561	154.69
ILE_658@HG22	GLN_174@HE21	GLN_174@NE2	0.0118	2.8359	143.9562
ILE_658@O	GLY_170@H	GLY_170@N	0.0118	2.9043	145.4256
SER_449@HG	GLN_77@HA	GLN_77@CA	0.0115	2.9165	142.1307
ASP_693@OD2	LYS_112@HZ2	LYS_112@NZ	0.0114	2.8069	158.9852
ILE_658@HG12	GLN_174@HE21	GLN_174@NE2	0.0109	2.8681	143.7305
ALA_659@HA	PRO_167@HA	PRO_167@CA	0.0108	2.931	144.078
ALA_659@O	TYR_173@H	TYR_173@N	0.0107	2.8773	149.4746
GLY_660@HA2	TYR_173@HB3	TYR_173@CB	0.0102	2.9298	142.4943

ARG_322@HH22	ARG_71@HE	ARG_71@NE	0.0102	2.9001	142.5842
LEU_691@HG	PRO_167@HD3	PRO_167@CD	0.0093	2.9391	144.9276

10.4.5.4. Determination of the interface interactions of the S protein (BA.4)-ACE2 and (S protein (BA.2.12.1)-ACE2 complexes.

An interface area is usually defined as a region where two sets of proteins come in contact with each other. Surface residues with large surface regions accessible to the solvent available usually characterize them. The interface statistics was obtained upon the submission of the corresponding lowest energy structure for both the complex (S protein (BA.4)-ACE2 and S protein (BA.2.12.1)-ACE2 complexes) from the 100 ns MD simulation trajectory using RMSD clustering algorithm using the PDBsum server. The interface statistics for both the complexes have been summarised in **Table 10.9.**

Table 10.9. *Interface statistics for the S protein (BA.4)-ACE2 and S protein (BA.2.12.1)-ACE2 complexes.*

Complex system	**Chain**	**No. of interface residue**	**Interface area (Å^2)**	**No. of salt bridge**	**No. of hydrogen bonds**	**No. of non-bonded contacts**
S Protein (BA4-ACE2)	SPIKE (BA.4)	30	1492	1	13	192
	ACE2	31	1523			
S Protein (BA2.12.1-ACE2)	SPIKE (BA.2.12.1)	35	1651	2	21	244
	ACE2	40	1595			

From **Table 10.9**, the total number of interface residues in the S protein (BA.4)-ACE2 and S protein (BA.2.12.1)-ACE2 complexes were found to be sixty-one and seventy-five, respectively. In the S protein (BA.4)-ACE2 complex, the interface area for the S protein chain and the ACE2 chain involved in the interaction was observed to be 1492 Å^2 and 1523 Å^2 respectively, while in the S protein (BA.2.12.1)-ACE2 complex, it was observed to be 1651 Å^2 and 1595 Å2 respectively. Both the BA.4 and BA.2.12.1 complexes were stabilized by molecular interactions like salt bridges, hydrogen bonding, and non-bonded contacts. **Table 10.9** shows the presence of one hundred and ninety-two non-bonded contacts, one salt bridge, and thirteen hydrogen bonds at the interface of S protein and ACE2 in the S protein (BA.4)-ACE2 complex. However, for the S protein (BA.2.12.1)-ACE2 complex, we

observed two hundred and forty-four non-bonded contacts, two salt bridges, and twenty-one hydrogen bonds at the S protein and ACE2 interface. Overall, the number of intermolecular interactions and the interface area shared by S protein and ACE2 in forming complex is larger in BA.2.12.1 complex than in the BA.4 type complex. Therefore, the stability of BA.2.12.1 complex was found to be higher than that of the BA.4 type complex.

The detailed contributions of each interface residue stabilizing the complexes were summarized in **Table 10.10, 10.11, 10.12** for BA.4 and **10.13, 10.14, 10.15** for BA.2.12.1.

Table 10.10. *List of atom-atom interactions (Salt bridges) across protein-ligand interface in Spike Protein (BA.2.12.1) (Chain A) and ACE2 receptor (Chain B) complex from PDBsum server*

Spike Protein (BA.2.12.1)						Salt brigdes	ACE2 receptor					
Sl. no.	Atom no.	Atom name	Res name	Res no.	Chain		Atom no.	Atom name	Res name	Res no.	Chain	Distance
1	730	OE2	GLU	406	A	<-->	7462	NE	ARG	582	B	3.65
2	1583	NH1	ARG	493	A	<-->	4047	OE1	GLU	232	B	2.59

Table 10.11. *List of atom-atom interactions (Hydrogen bonds) across protein-ligand interface in Spike Protein (BA.2.12.1) (Chain A) and ACE2 receptor (Chain B) complex from PDBsum server*

Spike Protein (BA.2.12.1)						Hydrogen bonds	ACE2 receptor					
Sl. no.	Atom no.	Atom name	Res name	Res no.	Chain		Atom no.	Atom name	Res name	Res no.	Chain	Distance
1	462	NZ	LYS	378	A	<-->	6981	OE1	GLN	531	B	2.66
2	722	O	ASN	405	A	<-->	7443	ND2	ASN	580	B	3.07
3	722	O	ASN	405	A	<-->	7468	NH2	ARG	582	B	2.67
4	745	OG	SER	408	A	<-->	6949	OE1	GLU	527	B	2.64
5	787	O	GLY	413	A	<-->	7035	N	GLY	537	B	2.77
6	804	OG1	THR	415	A	<-->	7039	O	GLY	537	B	2.8
7	804	OG1	THR	415	A	<-->	7047	N	LEU	539	B	3
8	814	N	ASN	417	A	<-->	7541	OE1	GLU	589	B	2.6
9	859	OH	TYR	421	A	<-->	7542	OE2	GLU	589	B	2.97
10	859	OH	TYR	421	A	<-->	7614	NZ	LYS	596	B	3.05
11	1179	OH	TYR	453	A	<-->	4047	OE1	GLU	232	B	2.89
12	1237	O	ARG	457	A	<-->	7614	NZ	LYS	596	B	2.83
13	1429	N	ASN	477	A	<-->	7664	O	LYS	600	B	2.63
14	1519	OD1	ASN	487	A	<-->	7696	N	VAL	604	B	2.78
15	1520	ND2	ASN	487	A	<-->	7683	O	SER	602	B	2.87
16	1542	OH	TYR	489	A	<-->	4109	OE1	GLU	238	B	2.62
17	1583	NH1	ARG	493	A	<-->	4040	O	GLU	231	B	3.16
18	1583	NH1	ARG	493	A	<-->	4047	OE1	GLU	232	B	2.59
19	1586	NH2	ARG	493	A	<-->	4040	O	GLU	231	B	3.27
20	1673	OH	TYR	501	A	<-->	3968	OE2	GLU	224	B	2.8
21	1703	NE2	HIS	505	A	<-->	7436	O	MET	579	B	2.87

Table 10.12. *List of atom-atom interactions (non-bonded contacts) across protein-ligand interface in Spike Protein (BA.2.12.1) (Chain A) and ACE2 receptor (Chain B) complex from PDBsum server*

Spike Protein (BA.2.12.1)						Non-bonded contacts	ACE2 receptor					
Sl. no.	Atom no.	Atom name	Res name	Res no.	Chain		Atom no.	Atom name	Res name	Res no.	Chain	Distance
1	460	CD	LYS	378	A	<-->	6981	OE1	GLN	531	B	3.74
2	461	CE	LYS	378	A	<-->	6981	OE1	GLN	531	B	3.45
3	462	NZ	LYS	378	A	<-->	6985	C	GLN	531	B	3.79
4	462	NZ	LYS	378	A	<-->	6986	O	GLN	531	B	3.14
5	462	NZ	LYS	378	A	<-->	6980	CD	GLN	531	B	3.87
6	462	NZ	LYS	378	A	<-->	6981	OE1	GLN	531	B	2.66
7	462	NZ	LYS	378	A	<-->	6987	N	ALA	532	B	3.88
8	462	NZ	LYS	378	A	<-->	6989	CA	ALA	532	B	3.28
9	462	NZ	LYS	378	A	<-->	6990	CB	ALA	532	B	3.88
10	482	CE1	TYR	380	A	<-->	7003	CG	LYS	534	B	3.69
11	485	OH	TYR	380	A	<-->	6986	O	GLN	531	B	3.39
12	721	C	ASN	405	A	<-->	7468	NH2	ARG	582	B	3.75
13	722	O	ASN	405	A	<-->	7443	ND2	ASN	580	B	3.07
14	722	O	ASN	405	A	<-->	7462	NE	ARG	582	B	3.69
15	722	O	ASN	405	A	<-->	7464	CZ	ARG	582	B	3.6
16	722	O	ASN	405	A	<-->	7468	NH2	ARG	582	B	2.67
17	715	CB	ASN	405	A	<-->	7401	CB	ALA	576	B	3.37
18	716	CG	ASN	405	A	<-->	7401	CB	ALA	576	B	3.66
19	717	OD1	ASN	405	A	<-->	7392	O	VAL	574	B	3.59
20	717	OD1	ASN	405	A	<-->	7388	CB	VAL	574	B	3.63
21	717	OD1	ASN	405	A	<-->	7390	CG2	VAL	574	B	3.64
22	718	ND2	ASN	405	A	<-->	6911	CG	GLN	524	B	3.32
23	718	ND2	ASN	405	A	<-->	6912	CD	GLN	524	B	3.38
24	718	ND2	ASN	405	A	<-->	6914	NE2	GLN	524	B	3.02
25	718	ND2	ASN	405	A	<-->	7440	CB	ASN	580	B	3.11
26	718	ND2	ASN	405	A	<-->	7441	CG	ASN	580	B	3.83
27	718	ND2	ASN	405	A	<-->	7443	ND2	ASN	580	B	3.5
28	725	CA	GLU	406	A	<-->	7468	NH2	ARG	582	B	3.81
29	727	CG	GLU	406	A	<-->	7462	NE	ARG	582	B	3.39
30	730	OE2	GLU	406	A	<-->	7461	CD	ARG	582	B	3.34
31	730	OE2	GLU	406	A	<-->	7462	NE	ARG	582	B	3.65
32	743	CA	SER	408	A	<-->	6979	CG	GLN	531	B	3.75
33	743	CA	SER	408	A	<-->	6982	NE2	GLN	531	B	3.27
34	748	O	SER	408	A	<-->	6978	CB	GLN	531	B	3.81
35	748	O	SER	408	A	<-->	6979	CG	GLN	531	B	3.31
36	744	CB	SER	408	A	<-->	6949	OE1	GLU	527	B	3.41
37	744	CB	SER	408	A	<-->	6982	NE2	GLN	531	B	3.73
38	745	OG	SER	408	A	<-->	6948	CD	GLU	527	B	3.73
39	745	OG	SER	408	A	<-->	6949	OE1	GLU	527	B	2.64
40	745	OG	SER	408	A	<-->	7468	NH2	ARG	582	B	3.39
41	753	CG	GLN	409	A	<-->	7464	CZ	ARG	582	B	3.55
42	753	CG	GLN	409	A	<-->	7465	NH1	ARG	582	B	3.52

43	753	CG	GLN	409	A	<-->	7468	NH2	ARG	582	B	3.88
44	754	CD	GLN	409	A	<-->	7464	CZ	ARG	582	B	3.67
45	754	CD	GLN	409	A	<-->	7465	NH1	ARG	582	B	3.11
46	755	OE1	GLN	409	A	<-->	7461	CD	ARG	582	B	3.73
47	755	OE1	GLN	409	A	<-->	7464	CZ	ARG	582	B	3.84
48	755	OE1	GLN	409	A	<-->	7465	NH1	ARG	582	B	3.21
49	756	NE2	GLN	409	A	<-->	6950	OE2	GLU	527	B	3.54
50	756	NE2	GLN	409	A	<-->	7465	NH1	ARG	582	B	3.45
51	756	NE2	GLN	409	A	<-->	7504	ND2	ASN	586	B	3.32
52	773	CB	ALA	411	A	<-->	6979	CG	GLN	531	B	3.9
53	777	CA	PRO	412	A	<-->	7031	OE1	GLU	536	B	3.69
54	781	C	PRO	412	A	<-->	7030	CD	GLU	536	B	3.84
55	781	C	PRO	412	A	<-->	7031	OE1	GLU	536	B	3.03
56	782	O	PRO	412	A	<-->	7024	O	HIS	535	B	3.84
57	782	O	PRO	412	A	<-->	7030	CD	GLU	536	B	3.76
58	782	O	PRO	412	A	<-->	7031	OE1	GLU	536	B	3.31
59	782	O	PRO	412	A	<-->	7032	OE2	GLU	536	B	3.7
60	778	CB	PRO	412	A	<-->	7031	OE1	GLU	536	B	3.17
61	783	N	GLY	413	A	<-->	7030	CD	GLU	536	B	3.9
62	783	N	GLY	413	A	<-->	7031	OE1	GLU	536	B	3.04
63	785	CA	GLY	413	A	<-->	7024	O	HIS	535	B	3.76
64	785	CA	GLY	413	A	<-->	7027	CA	GLU	536	B	3.08
65	785	CA	GLY	413	A	<-->	7033	C	GLU	536	B	3.83
66	785	CA	GLY	413	A	<-->	7028	CB	GLU	536	B	3.6
67	785	CA	GLY	413	A	<-->	7030	CD	GLU	536	B	3.79
68	785	CA	GLY	413	A	<-->	7031	OE1	GLU	536	B	3.32
69	785	CA	GLY	413	A	<-->	7035	N	GLY	537	B	3.52
70	786	C	GLY	413	A	<-->	7024	O	HIS	535	B	3.53
71	786	C	GLY	413	A	<-->	7027	CA	GLU	536	B	3.7
72	786	C	GLY	413	A	<-->	7035	N	GLY	537	B	3.39
73	787	O	GLY	413	A	<-->	7033	C	GLU	536	B	3.73
74	787	O	GLY	413	A	<-->	7035	N	GLY	537	B	2.77
75	787	O	GLY	413	A	<-->	7037	CA	GLY	537	B	3.47
76	787	O	GLY	413	A	<-->	7038	C	GLY	537	B	3.57
77	787	O	GLY	413	A	<-->	7039	O	GLY	537	B	3.04
78	788	N	GLN	414	A	<-->	7024	O	HIS	535	B	3.59
79	793	CD	GLN	414	A	<-->	7024	O	HIS	535	B	3.81
80	795	NE2	GLN	414	A	<-->	6972	O	CYS	530	B	3.53
81	795	NE2	GLN	414	A	<-->	6977	CA	GLN	531	B	3.62
82	795	NE2	GLN	414	A	<-->	7012	N	HIS	535	B	3.82
83	795	NE2	GLN	414	A	<-->	7024	O	HIS	535	B	3.25
84	807	C	THR	415	A	<-->	7502	CG	ASN	586	B	3.84
85	807	C	THR	415	A	<-->	7503	OD1	ASN	586	B	3.32
86	808	O	THR	415	A	<-->	7502	CG	ASN	586	B	3.23
87	808	O	THR	415	A	<-->	7503	OD1	ASN	586	B	3.07
88	808	O	THR	415	A	<-->	7504	ND2	ASN	586	B	3.14
89	803	CB	THR	415	A	<-->	7039	O	GLY	537	B	3.79
90	803	CB	THR	415	A	<-->	7041	CA	PRO	538	B	3.87
91	804	OG1	THR	415	A	<-->	7038	C	GLY	537	B	3.45
92	804	OG1	THR	415	A	<-->	7039	O	GLY	537	B	2.8

93	804	OG1	THR	415	A	<-->	7040	N	PRO	538	B	3.52
94	804	OG1	THR	415	A	<-->	7041	CA	PRO	538	B	2.94
95	804	OG1	THR	415	A	<-->	7045	C	PRO	538	B	3.36
96	804	OG1	THR	415	A	<-->	7047	N	LEU	539	B	3
97	804	OG1	THR	415	A	<-->	7503	OD1	ASN	586	B	3.82
98	806	CG2	THR	415	A	<-->	7038	C	GLY	537	B	3.8
99	806	CG2	THR	415	A	<-->	7039	O	GLY	537	B	3.69
100	806	CG2	THR	415	A	<-->	7040	N	PRO	538	B	3.87
101	806	CG2	THR	415	A	<-->	7041	CA	PRO	538	B	3.89
102	809	N	GLY	416	A	<-->	7503	OD1	ASN	586	B	3.53
103	811	CA	GLY	416	A	<-->	7500	CA	ASN	586	B	3.77
104	811	CA	GLY	416	A	<-->	7502	CG	ASN	586	B	3.72
105	811	CA	GLY	416	A	<-->	7503	OD1	ASN	586	B	3.49
106	811	CA	GLY	416	A	<-->	7539	CG	GLU	589	B	3.56
107	811	CA	GLY	416	A	<-->	7541	OE1	GLU	589	B	3.4
108	812	C	GLY	416	A	<-->	7541	OE1	GLU	589	B	3.47
109	814	N	ASN	417	A	<-->	7540	CD	GLU	589	B	3.51
110	814	N	ASN	417	A	<-->	7541	OE1	GLU	589	B	2.6
111	816	CA	ASN	417	A	<-->	7541	OE1	GLU	589	B	3.46
112	820	ND2	ASN	417	A	<-->	7494	CD1	LEU	585	B	3.39
113	829	CG1	ILE	418	A	<-->	7461	CD	ARG	582	B	3.52
114	843	CB	ASP	420	A	<-->	7539	CG	GLU	589	B	3.79
115	844	CG	ASP	420	A	<-->	7539	CG	GLU	589	B	3.72
116	846	OD2	ASP	420	A	<-->	7538	CB	GLU	589	B	3.83
117	846	OD2	ASP	420	A	<-->	7539	CG	GLU	589	B	3.22
118	857	CE2	TYR	421	A	<-->	7540	CD	GLU	589	B	3.77
119	857	CE2	TYR	421	A	<-->	7542	OE2	GLU	589	B	3.11
120	858	CZ	TYR	421	A	<-->	7542	OE2	GLU	589	B	3.23
121	858	CZ	TYR	421	A	<-->	7614	NZ	LYS	596	B	3.86
122	859	OH	TYR	421	A	<-->	7542	OE2	GLU	589	B	2.97
123	859	OH	TYR	421	A	<-->	7579	CG2	THR	593	B	3.67
124	859	OH	TYR	421	A	<-->	7614	NZ	LYS	596	B	3.05
125	919	CA	ASP	427	A	<-->	7031	OE1	GLU	536	B	3.23
126	924	C	ASP	427	A	<-->	7031	OE1	GLU	536	B	3.45
127	925	O	ASP	427	A	<-->	7030	CD	GLU	536	B	3.66
128	925	O	ASP	427	A	<-->	7031	OE1	GLU	536	B	2.91
129	920	CB	ASP	427	A	<-->	7028	CB	GLU	536	B	3.64
130	920	CB	ASP	427	A	<-->	7031	OE1	GLU	536	B	3.57
131	923	OD2	ASP	427	A	<-->	7027	CA	GLU	536	B	3.74
132	923	OD2	ASP	427	A	<-->	7028	CB	GLU	536	B	3.28
133	923	OD2	ASP	427	A	<-->	7035	N	GLY	537	B	3.49
134	1179	OH	TYR	453	A	<-->	4046	CD	GLU	232	B	3.34
135	1179	OH	TYR	453	A	<-->	4047	OE1	GLU	232	B	2.89
136	1179	OH	TYR	453	A	<-->	4048	OE2	GLU	232	B	3.18
137	1205	CD1	LEU	455	A	<-->	4047	OE1	GLU	232	B	3.4
138	1218	CZ	PHE	456	A	<-->	4075	CB	PRO	235	B	3.75
139	1218	CZ	PHE	456	A	<-->	4076	CG	PRO	235	B	3.57
140	1237	O	ARG	457	A	<-->	7614	NZ	LYS	596	B	2.83
141	1250	O	LYS	458	A	<-->	7579	CG2	THR	593	B	3.26
142	1250	O	LYS	458	A	<-->	7614	NZ	LYS	596	B	3.53

143	1400	CE2	TYR	473	A	<-->	7612	CD	LYS	596	B	3.5
144	1401	CZ	TYR	473	A	<-->	7612	CD	LYS	596	B	3.66
145	1402	OH	TYR	473	A	<-->	7610	CB	LYS	596	B	3.51
146	1402	OH	TYR	473	A	<-->	7611	CG	LYS	596	B	3.85
147	1402	OH	TYR	473	A	<-->	7612	CD	LYS	596	B	3.14
148	1402	OH	TYR	473	A	<-->	7613	CE	LYS	596	B	3.31
149	1402	OH	TYR	473	A	<-->	7614	NZ	LYS	596	B	3.41
150	1423	O	ALA	475	A	<-->	7651	O	ASN	599	B	3.54
151	1423	O	ALA	475	A	<-->	7654	CA	LYS	600	B	3.5
152	1423	O	ALA	475	A	<-->	7701	CG2	VAL	604	B	3.73
153	1421	CB	ALA	475	A	<-->	4120	CE1	HIS	239	B	3.81
154	1421	CB	ALA	475	A	<-->	4121	NE2	HIS	239	B	3.58
155	1426	CA	GLY	476	A	<-->	7654	CA	LYS	600	B	3.87
156	1426	CA	GLY	476	A	<-->	7663	C	LYS	600	B	3.79
157	1426	CA	GLY	476	A	<-->	7664	O	LYS	600	B	2.95
158	1427	C	GLY	476	A	<-->	7663	C	LYS	600	B	3.87
159	1427	C	GLY	476	A	<-->	7664	O	LYS	600	B	3.03
160	1429	N	ASN	477	A	<-->	7663	C	LYS	600	B	3.61
161	1429	N	ASN	477	A	<-->	7664	O	LYS	600	B	2.63
162	1431	CA	ASN	477	A	<-->	7664	O	LYS	600	B	3.62
163	1432	CB	ASN	477	A	<-->	7664	O	LYS	600	B	3.57
164	1432	CB	ASN	477	A	<-->	7667	CA	ASN	601	B	3.87
165	1433	CG	ASN	477	A	<-->	7664	O	LYS	600	B	3.65
166	1433	CG	ASN	477	A	<-->	7667	CA	ASN	601	B	3.61
167	1434	OD1	ASN	477	A	<-->	7664	O	LYS	600	B	3.29
168	1434	OD1	ASN	477	A	<-->	7667	CA	ASN	601	B	3.79
169	1435	ND2	ASN	477	A	<-->	7667	CA	ASN	601	B	3.9
170	1507	CD1	PHE	486	A	<-->	7691	CE1	PHE	603	B	3.86
171	1507	CD1	PHE	486	A	<-->	7693	CZ	PHE	603	B	3.75
172	1507	CD1	PHE	486	A	<-->	7703	O	VAL	604	B	3.77
173	1509	CE1	PHE	486	A	<-->	7688	CG	PHE	603	B	3.88
174	1509	CE1	PHE	486	A	<-->	7690	CD2	PHE	603	B	3.57
175	1509	CE1	PHE	486	A	<-->	7692	CE2	PHE	603	B	3.6
176	1509	CE1	PHE	486	A	<-->	7702	C	VAL	604	B	3.41
177	1509	CE1	PHE	486	A	<-->	7703	O	VAL	604	B	3.21
178	1509	CE1	PHE	486	A	<-->	7704	N	GLY	605	B	3.5
179	1509	CE1	PHE	486	A	<-->	7706	CA	GLY	605	B	3.46
180	1511	CZ	PHE	486	A	<-->	7703	O	VAL	604	B	3.66
181	1511	CZ	PHE	486	A	<-->	7704	N	GLY	605	B	3.76
182	1511	CZ	PHE	486	A	<-->	7706	CA	GLY	605	B	3.16
183	1511	CZ	PHE	486	A	<-->	7707	C	GLY	605	B	3.78
184	1518	CG	ASN	487	A	<-->	7696	N	VAL	604	B	3.58
185	1518	CG	ASN	487	A	<-->	7699	CB	VAL	604	B	3.87
186	1518	CG	ASN	487	A	<-->	7701	CG2	VAL	604	B	3.6
187	1519	OD1	ASN	487	A	<-->	7694	C	PHE	603	B	3.79
188	1519	OD1	ASN	487	A	<-->	7696	N	VAL	604	B	2.78
189	1519	OD1	ASN	487	A	<-->	7698	CA	VAL	604	B	3.46
190	1519	OD1	ASN	487	A	<-->	7702	C	VAL	604	B	3.89
191	1519	OD1	ASN	487	A	<-->	7703	O	VAL	604	B	3.85
192	1519	OD1	ASN	487	A	<-->	7699	CB	VAL	604	B	3.37

193	1519	OD1	ASN	487	A	<-->	7701	CG2	VAL	604	B	3.54
194	1520	ND2	ASN	487	A	<-->	7683	O	SER	602	B	2.87
195	1520	ND2	ASN	487	A	<-->	7696	N	VAL	604	B	3.7
196	1520	ND2	ASN	487	A	<-->	7701	CG2	VAL	604	B	3.52
197	1539	CE1	TYR	489	A	<-->	4109	OE1	GLU	238	B	3.63
198	1540	CE2	TYR	489	A	<-->	4109	OE1	GLU	238	B	3.87
199	1541	CZ	TYR	489	A	<-->	4109	OE1	GLU	238	B	3.13
200	1542	OH	TYR	489	A	<-->	4108	CD	GLU	238	B	3.82
201	1542	OH	TYR	489	A	<-->	4109	OE1	GLU	238	B	2.62
202	1542	OH	TYR	489	A	<-->	7703	O	VAL	604	B	3.79
203	1542	OH	TYR	489	A	<-->	7699	CB	VAL	604	B	3.72
204	1542	OH	TYR	489	A	<-->	7700	CG1	VAL	604	B	3.36
205	1579	CD	ARG	493	A	<-->	4047	OE1	GLU	232	B	3.33
206	1582	CZ	ARG	493	A	<-->	4040	O	GLU	231	B	3.67
207	1582	CZ	ARG	493	A	<-->	4047	OE1	GLU	232	B	3.65
208	1583	NH1	ARG	493	A	<-->	4039	C	GLU	231	B	3.74
209	1583	NH1	ARG	493	A	<-->	4040	O	GLU	231	B	3.16
210	1583	NH1	ARG	493	A	<-->	4041	N	GLU	232	B	3.87
211	1583	NH1	ARG	493	A	<-->	4043	CA	GLU	232	B	3.43
212	1583	NH1	ARG	493	A	<-->	4045	CG	GLU	232	B	3.61
213	1583	NH1	ARG	493	A	<-->	4046	CD	GLU	232	B	3.49
214	1583	NH1	ARG	493	A	<-->	4047	OE1	GLU	232	B	2.59
215	1586	NH2	ARG	493	A	<-->	4040	O	GLU	231	B	3.27
216	1586	NH2	ARG	493	A	<-->	4076	CG	PRO	235	B	3.88
217	1668	CD1	TYR	501	A	<-->	7423	ND2	ASN	578	B	3.89
218	1670	CE1	TYR	501	A	<-->	3938	NE2	GLN	221	B	3.55
219	1670	CE1	TYR	501	A	<-->	3968	OE2	GLU	224	B	3.63
220	1670	CE1	TYR	501	A	<-->	3976	OD1	ASP	225	B	3.61
221	1672	CZ	TYR	501	A	<-->	3968	OE2	GLU	224	B	3.42
222	1673	OH	TYR	501	A	<-->	3966	CD	GLU	224	B	3.72
223	1673	OH	TYR	501	A	<-->	3968	OE2	GLU	224	B	2.8
224	1679	CA	GLY	502	A	<-->	7407	CB	LYS	577	B	3.71
225	1682	N	VAL	503	A	<-->	7404	N	LYS	577	B	3.82
226	1682	N	VAL	503	A	<-->	7407	CB	LYS	577	B	3.58
227	1682	N	VAL	503	A	<-->	7409	CD	LYS	577	B	3.6
228	1685	CB	VAL	503	A	<-->	7362	OE1	GLU	571	B	2.89
229	1686	CG1	VAL	503	A	<-->	7362	OE1	GLU	571	B	3.5
230	1686	CG1	VAL	503	A	<-->	7397	O	GLY	575	B	3.45
231	1687	CG2	VAL	503	A	<-->	7361	CD	GLU	571	B	3.88
232	1687	CG2	VAL	503	A	<-->	7362	OE1	GLU	571	B	3.14
233	1687	CG2	VAL	503	A	<-->	7409	CD	LYS	577	B	3.75
234	1687	CG2	VAL	503	A	<-->	7410	CE	LYS	577	B	3.46
235	1687	CG2	VAL	503	A	<-->	7411	NZ	LYS	577	B	3.62
236	1690	N	GLY	504	A	<-->	7400	CA	ALA	576	B	3.71
237	1690	N	GLY	504	A	<-->	7401	CB	ALA	576	B	3.58
238	1690	N	GLY	504	A	<-->	7404	N	LYS	577	B	3.56
239	1692	CA	GLY	504	A	<-->	7401	CB	ALA	576	B	3.26
240	1701	CD2	HIS	505	A	<-->	7420	CB	ASN	578	B	3.7
241	1701	CD2	HIS	505	A	<-->	7423	ND2	ASN	578	B	3.73
242	1701	CD2	HIS	505	A	<-->	7436	O	MET	579	B	3.79

243	1702	CE1	HIS	505	A	<-->	7436	O	MET	579	B	3.77
244	1703	NE2	HIS	505	A	<-->	7436	O	MET	579	B	2.87

Table 10.13. *List of atom-atom interactions (Salt bridges) across protein-ligand interface in Spike Protein (BA.4) (Chain A) and ACE2 receptor (Chain B) complex from PDBsum server*

Spike Protein (BA.4)						Salt bridges	ACE2 receptor					
Sl.no	Atom no.	Atom name	Res name	Res no.	Chain		Atom no.	Atom name	Res name	Res no.	Chain	Distance
1	699	NH1	ARG	403	A	<-->	7538	OE2	GLU	589	B	2.66

Table 10.14. *List of atom-atom interactions (Hydrogen bonds) across protein-ligand interface in Spike Protein (BA.4) (Chain A) and ACE2 receptor (Chain B) complex from PDBsum server*

Spike Protein (BA.4)						Hydrogen bonds	ACE2 receptor					
Sl. no	Atom no.	Atom name	Res name	Res no.	Chain		Atom no.	Atom name	Res name	Res no.	Chain	Distance
1	699	NH1	ARG	403	A	<-->	7537	OE1	GLU	589	B	2.66
2	702	NH2	ARG	403	A	<-->	7499	OD1	ASN	586	B	2.67
3	718	ND2	ASN	405	A	<-->	7035	O	GLY	537	B	3.03
4	756	NE2	GLN	409	A	<-->	7538	OE2	GLU	589	B	2.7
5	814	N	ASN	417	A	<-->	7538	OE2	GLU	589	B	3.19
6	819	OD1	ASN	417	A	<-->	7610	NZ	LYS	596	B	2.69
7	846	OD2	ASP	420	A	<-->	7573	OG1	THR	593	B	3.05
8	1213	O	LEU	455	A	<-->	7610	NZ	LYS	596	B	2.9
9	1260	OG	SER	459	A	<-->	7660	O	LYS	600	B	2.68
10	1440	ND2	ASN	477	A	<-->	7743	OD1	ASP	609	B	2.73
11	1582	NE2	GLN	493	A	<-->	4044	OE2	GLU	232	B	2.81
12	1635	NH1	ARG	498	A	<-->	7393	O	GLY	575	B	2.73
13	1732	OH	TYR	508	A	<-->	7028	OE2	GLU	536	B	2.68

Table 10.15. *List of atom-atom interactions (Non-bonded contacts) across protein-ligand interface in Spike Protein (BA.4) (Chain A) and ACE2 receptor (Chain B) complex from PDBsum server*

Spike Protein(BA.4)						Non-bonded contacts	ACE2 receptor					
Sl. no.	Atom no.	Atom name	Res name	Res no.	Chain		Atom no.	Atom name	Res name	Res no.	Chain	Distance
1	698	CZ	ARG	403	A	<-->	7499	OD1	ASN	586	B	3.85
2	698	CZ	ARG	403	A	<-->	7537	OE1	GLU	589	B	3.5
3	699	NH1	ARG	403	A	<-->	7535	CG	GLU	589	B	3.81
4	699	NH1	ARG	403	A	<-->	7536	CD	GLU	589	B	3.48
5	699	NH1	ARG	403	A	<-->	7537	OE1	GLU	589	B	2.66
6	702	NH2	ARG	403	A	<-->	7498	CG	ASN	586	B	3.54
7	702	NH2	ARG	403	A	<-->	7499	OD1	ASN	586	B	2.67
8	702	NH2	ARG	403	A	<-->	7537	OE1	GLU	589	B	3.47
9	716	CG	ASN	405	A	<-->	7034	C	GLY	537	B	3.39

10	716	CG	ASN	405	A	<-->	7035	O	GLY	537	B	3.19
11	716	CG	ASN	405	A	<-->	7036	N	PRO	538	B	3.8
12	717	OD1	ASN	405	A	<-->	7031	N	GLY	537	B	3.42
13	717	OD1	ASN	405	A	<-->	7033	CA	GLY	537	B	3.59
14	717	OD1	ASN	405	A	<-->	7034	C	GLY	537	B	3.24
15	717	OD1	ASN	405	A	<-->	7035	O	GLY	537	B	2.89
16	718	ND2	ASN	405	A	<-->	7034	C	GLY	537	B	3.41
17	718	ND2	ASN	405	A	<-->	7035	O	GLY	537	B	3.03
18	718	ND2	ASN	405	A	<-->	7036	N	PRO	538	B	3.56
19	718	ND2	ASN	405	A	<-->	7037	CA	PRO	538	B	3.36
20	718	ND2	ASN	405	A	<-->	7041	C	PRO	538	B	3.72
21	718	ND2	ASN	405	A	<-->	7043	N	LEU	539	B	3.49
22	718	ND2	ASN	405	A	<-->	7499	OD1	ASN	586	B	3.56
23	727	CG	GLU	406	A	<-->	7537	OE1	GLU	589	B	3.75
24	754	CD	GLN	409	A	<-->	7538	OE2	GLU	589	B	3.47
25	755	OE1	GLN	409	A	<-->	7538	OE2	GLU	589	B	3.54
26	756	NE2	GLN	409	A	<-->	7536	CD	GLU	589	B	3.34
27	756	NE2	GLN	409	A	<-->	7537	OE1	GLU	589	B	3.23
28	756	NE2	GLN	409	A	<-->	7538	OE2	GLU	589	B	2.7
29	807	C	THR	415	A	<-->	7575	CG2	THR	593	B	3.39
30	808	O	THR	415	A	<-->	7575	CG2	THR	593	B	3.57
31	809	N	GLY	416	A	<-->	7575	CG2	THR	593	B	3.33
32	811	CA	GLY	416	A	<-->	7575	CG2	THR	593	B	3.51
33	812	C	GLY	416	A	<-->	7572	CB	THR	593	B	3.5
34	812	C	GLY	416	A	<-->	7573	OG1	THR	593	B	3.16
35	812	C	GLY	416	A	<-->	7575	CG2	THR	593	B	3.6
36	813	O	GLY	416	A	<-->	7572	CB	THR	593	B	3.73
37	813	O	GLY	416	A	<-->	7573	OG1	THR	593	B	2.92
38	814	N	ASN	417	A	<-->	7538	OE2	GLU	589	B	3.19
39	814	N	ASN	417	A	<-->	7572	CB	THR	593	B	3.57
40	814	N	ASN	417	A	<-->	7573	OG1	THR	593	B	3.45
41	816	CA	ASN	417	A	<-->	7538	OE2	GLU	589	B	3.8
42	816	CA	ASN	417	A	<-->	7573	OG1	THR	593	B	3.53
43	817	CB	ASN	417	A	<-->	7535	CG	GLU	589	B	3.65
44	817	CB	ASN	417	A	<-->	7536	CD	GLU	589	B	3.71
45	817	CB	ASN	417	A	<-->	7538	OE2	GLU	589	B	3.18
46	818	CG	ASN	417	A	<-->	7610	NZ	LYS	596	B	3.86
47	819	OD1	ASN	417	A	<-->	7609	CE	LYS	596	B	3.66
48	819	OD1	ASN	417	A	<-->	7610	NZ	LYS	596	B	2.69
49	820	ND2	ASN	417	A	<-->	7535	CG	GLU	589	B	3.51
50	843	CB	ASP	420	A	<-->	7573	OG1	THR	593	B	3.38
51	844	CG	ASP	420	A	<-->	7573	OG1	THR	593	B	3.66
52	846	OD2	ASP	420	A	<-->	7572	CB	THR	593	B	3.85
53	846	OD2	ASP	420	A	<-->	7573	OG1	THR	593	B	3.05

54	846	OD2	ASP	420	A	<-->	7575	CG2	THR	593	B	3.43
55	852	CB	TYR	421	A	<-->	7610	NZ	LYS	596	B	3.58
56	853	CG	TYR	421	A	<-->	7610	NZ	LYS	596	B	3.38
57	854	CD1	TYR	421	A	<-->	7610	NZ	LYS	596	B	3.9
58	855	CD2	TYR	421	A	<-->	7608	CD	LYS	596	B	3.81
59	855	CD2	TYR	421	A	<-->	7610	NZ	LYS	596	B	3.5
60	856	CE1	TYR	421	A	<-->	7606	CB	LYS	596	B	3.74
61	857	CE2	TYR	421	A	<-->	7608	CD	LYS	596	B	3.51
62	858	CZ	TYR	421	A	<-->	7606	CB	LYS	596	B	3.65
63	858	CZ	TYR	421	A	<-->	7608	CD	LYS	596	B	3.62
64	859	OH	TYR	421	A	<-->	7615	O	LYS	596	B	3.76
65	859	OH	TYR	421	A	<-->	7606	CB	LYS	596	B	3.51
66	1213	O	LEU	455	A	<-->	7565	CE2	PHE	592	B	3.76
67	1213	O	LEU	455	A	<-->	7608	CD	LYS	596	B	3.48
68	1213	O	LEU	455	A	<-->	7609	CE	LYS	596	B	3.72
69	1213	O	LEU	455	A	<-->	7610	NZ	LYS	596	B	2.9
70	1209	CG	LEU	455	A	<-->	7565	CE2	PHE	592	B	3.76
71	1210	CD1	LEU	455	A	<-->	7563	CD2	PHE	592	B	3.85
72	1210	CD1	LEU	455	A	<-->	7565	CE2	PHE	592	B	3.73
73	1221	CE1	PHE	456	A	<-->	4071	CB	PRO	235	B	3.27
74	1221	CE1	PHE	456	A	<-->	4072	CG	PRO	235	B	3.46
75	1223	CZ	PHE	456	A	<-->	4071	CB	PRO	235	B	3.86
76	1223	CZ	PHE	456	A	<-->	4072	CG	PRO	235	B	3.48
77	1255	O	LYS	458	A	<-->	7650	CA	LYS	600	B	3.88
78	1255	O	LYS	458	A	<-->	7660	O	LYS	600	B	3.58
79	1258	CA	SER	459	A	<-->	7660	O	LYS	600	B	3.69
80	1258	CA	SER	459	A	<-->	7651	CB	LYS	600	B	3.82
81	1259	CB	SER	459	A	<-->	7660	O	LYS	600	B	3.27
82	1260	OG	SER	459	A	<-->	7659	C	LYS	600	B	3.82
83	1260	OG	SER	459	A	<-->	7660	O	LYS	600	B	2.68
84	1264	N	ASN	460	A	<-->	7651	CB	LYS	600	B	3.63
85	1268	CG	ASN	460	A	<-->	7621	OD1	ASP	597	B	3.85
86	1268	CG	ASN	460	A	<-->	7653	CD	LYS	600	B	3.8
87	1269	OD1	ASN	460	A	<-->	7614	C	LYS	596	B	3.85
88	1269	OD1	ASN	460	A	<-->	7615	O	LYS	596	B	3.62
89	1269	OD1	ASN	460	A	<-->	7616	N	ASP	597	B	3.78
90	1269	OD1	ASN	460	A	<-->	7618	CA	ASP	597	B	3.42
91	1269	OD1	ASN	460	A	<-->	7651	CB	LYS	600	B	3.27
92	1269	OD1	ASN	460	A	<-->	7653	CD	LYS	600	B	3.71
93	1270	ND2	ASN	460	A	<-->	7618	CA	ASP	597	B	3.69
94	1270	ND2	ASN	460	A	<-->	7619	CB	ASP	597	B	3.58
95	1270	ND2	ASN	460	A	<-->	7620	CG	ASP	597	B	3.82
96	1270	ND2	ASN	460	A	<-->	7621	OD1	ASP	597	B	3.15
97	1425	CA	ALA	475	A	<-->	7699	O	VAL	604	B	3.28

98	1427	C	ALA	475	A	<-->	7689	CZ	PHE	603	B	3.88
99	1427	C	ALA	475	A	<-->	7699	O	VAL	604	B	3.42
100	1428	O	ALA	475	A	<-->	7688	CE2	PHE	603	B	3.43
101	1428	O	ALA	475	A	<-->	7689	CZ	PHE	603	B	3.19
102	1428	O	ALA	475	A	<-->	7698	C	VAL	604	B	3.65
103	1428	O	ALA	475	A	<-->	7699	O	VAL	604	B	2.79
104	1428	O	ALA	475	A	<-->	7700	N	GLY	605	B	3.83
105	1428	O	ALA	475	A	<-->	7702	CA	GLY	605	B	3.14
106	1426	CB	ALA	475	A	<-->	4104	CD	GLU	238	B	3.89
107	1426	CB	ALA	475	A	<-->	4106	OE2	GLU	238	B	3.3
108	1426	CB	ALA	475	A	<-->	7699	O	VAL	604	B	3.39
109	1433	O	GLY	476	A	<-->	7689	CZ	PHE	603	B	3.49
110	1434	N	ASN	477	A	<-->	7720	O	TRP	606	B	3.74
111	1438	CG	ASN	477	A	<-->	7723	CA	SER	607	B	3.71
112	1438	CG	ASN	477	A	<-->	7743	OD1	ASP	609	B	3.87
113	1439	OD1	ASN	477	A	<-->	7720	O	TRP	606	B	3.55
114	1439	OD1	ASN	477	A	<-->	7723	CA	SER	607	B	3.56
115	1439	OD1	ASN	477	A	<-->	7729	N	THR	608	B	3.66
116	1439	OD1	ASN	477	A	<-->	7733	OG1	THR	608	B	3.66
117	1440	ND2	ASN	477	A	<-->	7723	CA	SER	607	B	3.83
118	1440	ND2	ASN	477	A	<-->	7724	CB	SER	607	B	3.67
119	1440	ND2	ASN	477	A	<-->	7725	OG	SER	607	B	3.87
120	1440	ND2	ASN	477	A	<-->	7743	OD1	ASP	609	B	2.73
121	1506	O	GLY	485	A	<-->	4033	OE1	GLU	231	B	3.56
122	1518	CB	ASN	487	A	<-->	4106	OE2	GLU	238	B	3.53
123	1519	CG	ASN	487	A	<-->	4106	OE2	GLU	238	B	3.24
124	1520	OD1	ASN	487	A	<-->	4106	OE2	GLU	238	B	3.6
125	1521	ND2	ASN	487	A	<-->	4106	OE2	GLU	238	B	3.42
126	1538	CD1	TYR	489	A	<-->	4072	CG	PRO	235	B	3.89
127	1539	CD2	TYR	489	A	<-->	4036	O	GLU	231	B	3.77
128	1540	CE1	TYR	489	A	<-->	4072	CG	PRO	235	B	3.6
129	1541	CE2	TYR	489	A	<-->	4059	CB	LYS	234	B	3.68
130	1541	CE2	TYR	489	A	<-->	4072	CG	PRO	235	B	3.84
131	1541	CE2	TYR	489	A	<-->	4073	CD	PRO	235	B	3.71
132	1542	CZ	TYR	489	A	<-->	4069	N	PRO	235	B	3.78
133	1542	CZ	TYR	489	A	<-->	4070	CA	PRO	235	B	3.89
134	1542	CZ	TYR	489	A	<-->	4072	CG	PRO	235	B	3.57
135	1542	CZ	TYR	489	A	<-->	4073	CD	PRO	235	B	3.76
136	1543	OH	TYR	489	A	<-->	4067	C	LYS	234	B	3.77
137	1543	OH	TYR	489	A	<-->	4069	N	PRO	235	B	3.48
138	1543	OH	TYR	489	A	<-->	4070	CA	PRO	235	B	3.48
139	1543	OH	TYR	489	A	<-->	4103	CG	GLU	238	B	3.37
140	1582	NE2	GLN	493	A	<-->	4044	OE2	GLU	232	B	2.81
141	1613	O	GLY	496	A	<-->	7458	NE	ARG	582	B	3.65

142	1613	O	GLY	496	A	<-->	7464	NH2	ARG	582	B	3.65
143	1635	NH1	ARG	498	A	<-->	7392	C	GLY	575	B	3.63
144	1635	NH1	ARG	498	A	<-->	7393	O	GLY	575	B	2.73
145	1635	NH1	ARG	498	A	<-->	7394	N	ALA	576	B	3.84
146	1635	NH1	ARG	498	A	<-->	7396	CA	ALA	576	B	3.18
147	1658	O	THR	500	A	<-->	6975	CG	GLN	531	B	3.78
148	1658	O	THR	500	A	<-->	6976	CD	GLN	531	B	3.08
149	1658	O	THR	500	A	<-->	6977	OE1	GLN	531	B	3.37
150	1658	O	THR	500	A	<-->	6978	NE2	GLN	531	B	2.96
151	1654	OG1	THR	500	A	<-->	7393	O	GLY	575	B	3.74
152	1671	C	TYR	501	A	<-->	6974	CB	GLN	531	B	3.88
153	1664	CD1	TYR	501	A	<-->	6978	NE2	GLN	531	B	3.6
154	1665	CD2	TYR	501	A	<-->	7464	NH2	ARG	582	B	3.61
155	1666	CE1	TYR	501	A	<-->	6946	OE2	GLU	527	B	3.83
156	1666	CE1	TYR	501	A	<-->	7388	O	VAL	574	B	3.62
157	1667	CE2	TYR	501	A	<-->	7464	NH2	ARG	582	B	3.39
158	1668	CZ	TYR	501	A	<-->	7464	NH2	ARG	582	B	3.84
159	1673	N	GLY	502	A	<-->	6973	CA	GLN	531	B	3.63
160	1673	N	GLY	502	A	<-->	6974	CB	GLN	531	B	3.27
161	1673	N	GLY	502	A	<-->	6975	CG	GLN	531	B	3.81
162	1675	CA	GLY	502	A	<-->	6973	CA	GLN	531	B	3.43
163	1675	CA	GLY	502	A	<-->	6982	O	GLN	531	B	3.68
164	1675	CA	GLY	502	A	<-->	6974	CB	GLN	531	B	3.71
165	1680	CA	VAL	503	A	<-->	7028	OE2	GLU	536	B	3.78
166	1684	C	VAL	503	A	<-->	7028	OE2	GLU	536	B	3.12
167	1685	O	VAL	503	A	<-->	7028	OE2	GLU	536	B	3.31
168	1681	CB	VAL	503	A	<-->	7025	CG	GLU	536	B	3.8
169	1681	CB	VAL	503	A	<-->	7026	CD	GLU	536	B	3.77
170	1681	CB	VAL	503	A	<-->	7028	OE2	GLU	536	B	3.22
171	1683	CG2	VAL	503	A	<-->	6997	CA	LYS	534	B	3.79
172	1683	CG2	VAL	503	A	<-->	7006	C	LYS	534	B	3.52
173	1683	CG2	VAL	503	A	<-->	7007	O	LYS	534	B	3.5
174	1683	CG2	VAL	503	A	<-->	7020	O	HIS	535	B	3.85
175	1683	CG2	VAL	503	A	<-->	7025	CG	GLU	536	B	3.47
176	1683	CG2	VAL	503	A	<-->	7028	OE2	GLU	536	B	3.82
177	1686	N	GLY	504	A	<-->	7020	O	HIS	535	B	3.36
178	1686	N	GLY	504	A	<-->	7028	OE2	GLU	536	B	3.19
179	1688	CA	GLY	504	A	<-->	7020	O	HIS	535	B	3.8
180	1688	CA	GLY	504	A	<-->	7028	OE2	GLU	536	B	3.48
181	1696	ND1	HIS	505	A	<-->	7500	ND2	ASN	586	B	3.28
182	1697	CD2	HIS	505	A	<-->	6943	CG	GLU	527	B	3.54
183	1698	CE1	HIS	505	A	<-->	6943	CG	GLU	527	B	3.83
184	1698	CE1	HIS	505	A	<-->	7048	CD1	LEU	539	B	3.84
185	1698	CE1	HIS	505	A	<-->	7500	ND2	ASN	586	B	3.37

186	1699	NE2	HIS	505	A	<-->	6948	O	GLU	527	B	3.84
187	1699	NE2	HIS	505	A	<-->	6943	CG	GLU	527	B	3.4
188	1729	CE1	TYR	508	A	<-->	7028	OE2	GLU	536	B	3.78
189	1731	CZ	TYR	508	A	<-->	7028	OE2	GLU	536	B	3.38
190	1732	OH	TYR	508	A	<-->	7026	CD	GLU	536	B	3.2
191	1732	OH	TYR	508	A	<-->	7027	OE1	GLU	536	B	3.23
192	1732	OH	TYR	508	A	<-->	7028	OE2	GLU	536	B	2.68

The residues that were involved in the interaction between the RBD of S protein and ACE2 in the case of both the variants have been shown in **Figure 10.12**.

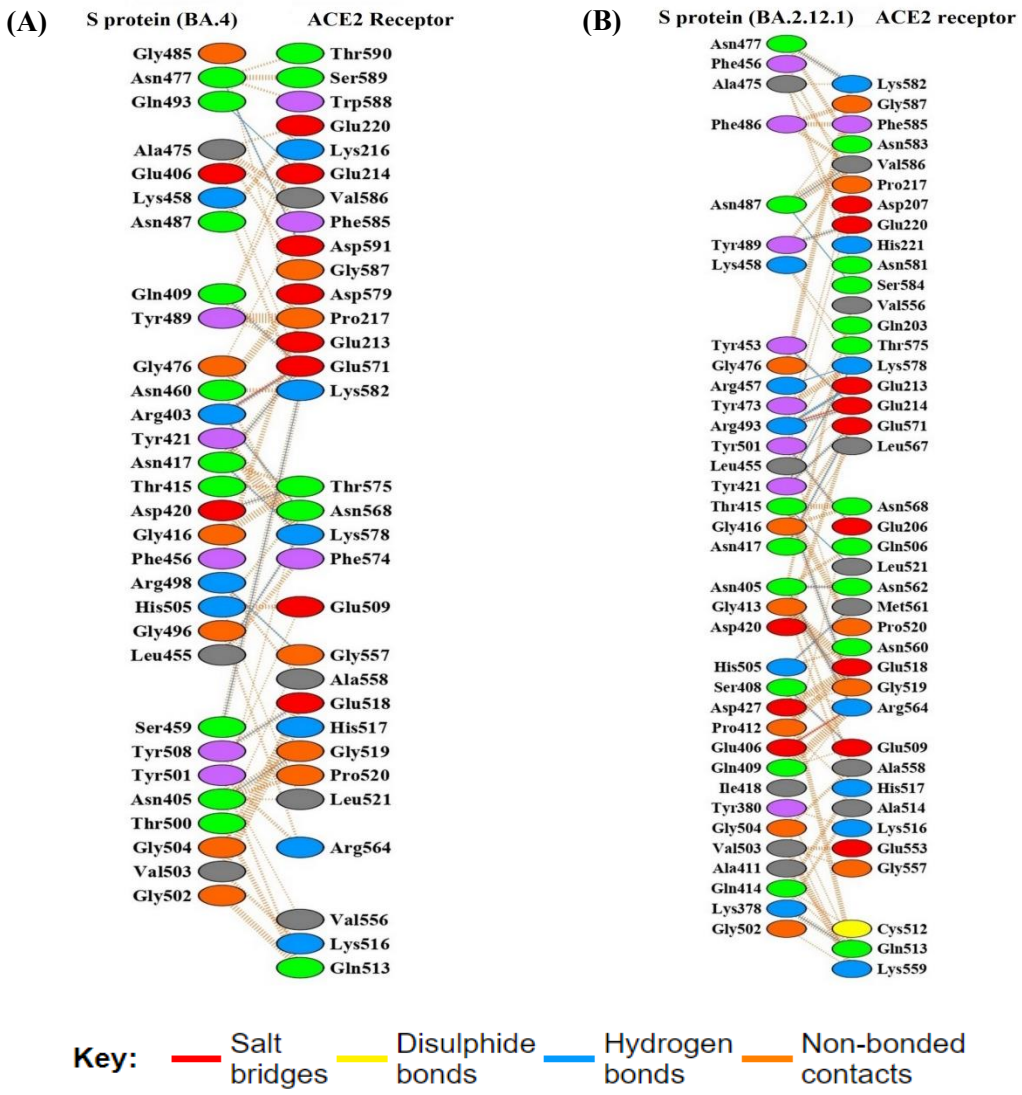

Figure 10.12. *Intermolecular interactions at residue level between ACE2 and S protein in* ***(A)*** *S protein (BA.4)-ACE2 and* ***(B)*** *S protein (BA.2.12.1) - ACE2 complex.*

10.4.5.5. Binding Free energy and per residue energy decomposition (PRED) analysis.

Once the system reached equilibrium, the binding free energy calculation was carried out for the S protein (BA.4)-ACE2 and S protein (BA.2.12.1)-ACE2 complexes from the last 10 ns of the MD simulation using MM-GBSA approach. As the MM-GBSA approach uses a continuum solvent approach to determine the binding free energies of a system, the values presented here only represent the relative binding free energy rather than the absolute or total binding energy. The binding free energies determined for the BA.4 and BA.2.12.1 complexes along with the energy terms, were summarized in **Table 10.16**. From the **Table 10.16**, it can be seen that S protein (BA.2.12.1)-ACE2 (ΔG_{bind} = -16.65 kcal/mol) complex was energetically more favourable than the S protein (BA.4)-ACE2 complex (ΔG_{bind} = -4.53 kcal/mol). Analysing **Table 10.16**, we observed that all the derived components for the BFE analysis contributed to the binding of S protein and ACE2 to form the S protein (BA.4 /BA.2.12.1)-ACE2 complex.

Table 10.16. *Binding free energies (kcal/mol) and its components of S protein (BA.4)-ACE2 and S protein (BA.2.12.1.12.1)-ACE2 complexes obtained using MM-GBSA approach.*

	$\Delta G_{(S\ protein(BA.4)-ACE2)} - [\Delta G_{S\ protein(BA.4)} + \Delta G_{ACE2}]$ (kcal/mol)		**$\Delta G_{(S\ protein(BA2.12.1)-ACE2)} - [\Delta G_{S\ protein(BA2.12.1)} + \Delta G_{ACE2}]$ (kcal/mol)**	
	average	**std. dev. (±)**	**average**	**std. dev. (±)**
VDW	-108.70	4.11	-92.74	21.74
ELE	-1474.47	21.42	-1413.07	17.10
GB	1582.38	21.22	1580.53	18.44
GBSUR	-12.28	0.37	-14.64	0.26
GAS	-1571.18	20.56	-1612.32	29.80
GBSOL	1570.10	21.26	1509.89	18.37
GBTOT	-7.07	2.99	-21.17	3.24
TΔS	-2.54	0.42	-4.52	1.12
ΔG_{bind}	**-4.53**		**-16.65**	

PRED values were determined to provide insight into each individual amino acid residue that were contributing to the overall PPI of the S protein (BA.4/BA.2.12.1)-ACE2 complexes. In this analysis, the total binding energy was decomposed into residues to identify key residues for ACE2 binding to S protein (BA.4/BA.2.12.1). Essential residues with the binding energy value below -1.00 kcal/mol were shown in the **Figure 10.13 and 10.14.** The highest energy contributions for S protein (BA.4) come from the residues ARG403, ALA475, VAL503, ASN417, PHE456, LEU455, TYR489, GLY502,

GLY504, HIE505 while in S protein (BA.2.12.1) come from the residues ASN460, SER459, ARG493, PHE456, ASP420, ASN487, PHE486, LEU461, TYR473, LYS424.

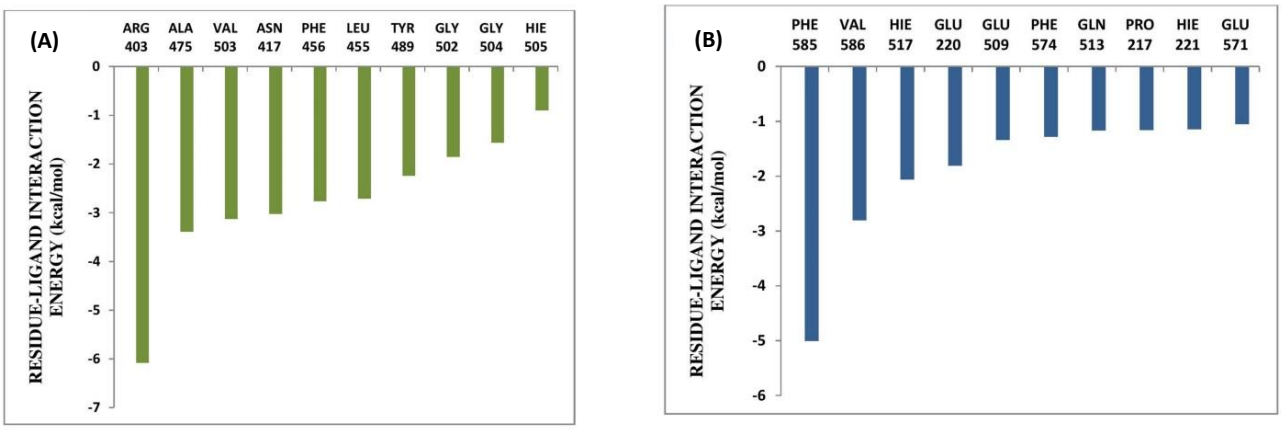

Figure 10.13. *Decomposition of binding free energy (kcal/mol) on per residue basis for* ***(A)*** *SPIKE (BA.4) and* ***(B)*** *ACE2 obtained using MM-GBSA approach*

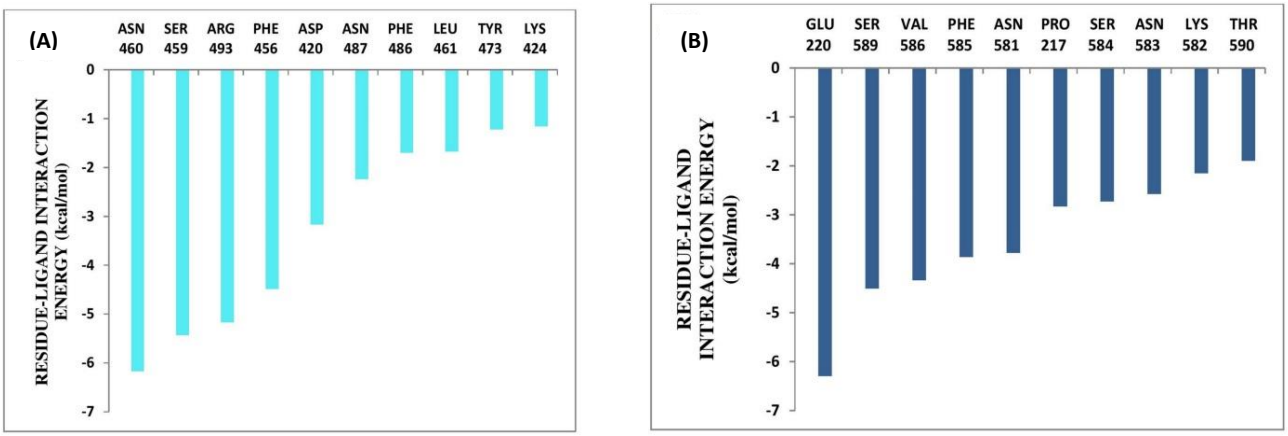

Figure 10.14. *Decomposition of binding free energy (kcal/mol) on per residue basis for* ***(A)*** *SPIKE (BA.2.12.1) and* ***(B)*** *ACE2 obtained using MM-GBSA approach*

Discussion: The structural and energetic insights of the study suggest that the BA.2.12.1 mutant complex exhibits higher stability which was shown by a reduced RMSD and RMSF values for the BA.2.12.1 mutant complex compared to the BA.4 mutant complex, particularly in and around the mutated residues. It was seen the mutated residues along with few residues around it attained higher stability in both the mutated complex which might be responsible for the stable and strong binding of the RBD of spike protein to the ACE2. Additionally, binding free energy and PRED analysis reflects light on the binding of the RBD to the ACE2 receptor in both the complex and results showed that the BA.2.12.1 complex had significantly more favourable energetics than the BA.4 and the PRED analysis provide us the residues in and around the mutation having the highest

contribution to the total binding energy hence supporting the possibility of increased infectivity in the mutated complex. The key interactive residues between the S protein and ACE2 in both complexes could serve as valuable targets for designing novel inhibitors or ligands against the disease. These interactions may also aid in developing broad-spectrum inhibitors effective against future coronavirus variants.

10.5. Conclusion:

It is difficult to conclude whether the SARS-CoV-2 BA.4 or BA.2.12.1 mutation is causing a more severe COVID-19 sickness than those variants seen during the initial wave of the COVID-19 pandemic. It is unclear if the higher mortality is due to one of the variants being more lethal than the other due to the mutations. The current study shows the effect of this BA.4 and BA.2.12.1 omicron variant on SARS-CoV-2 RBD towards its interaction with the ACE2 using MD simulation and other computational approaches. We observed significant structural changes in the mutation area of the spike protein in the S protein(BA.4)-ACE2 and S protein(BA.2.12.1)-ACE2 complexes from various analysis. From the secondary structure prediction analysis we observed BA.2.12.1 has a higher alpha helix and extended strand structure as compared to BA.4 which explains increase in stability of secondary structure in the BA.2.12.1 structure. The RMSD, RMSF, and inter-molecular hydrogen bond studies showed a similar pattern in case of the stabilty of the S protein (BA.2.12.1)-ACE2 complex over the S protein (BA.4)-ACE2 complex. The S protein(BA.2.12.1)-ACE2 complex was also shown to have a larger number of non-bonded interactions. Based on calculations of the binding free energies of the S protein(BA.4)-ACE2 and S protein(BA.2.12.1)-ACE2 complexes, we found that the affinity between S protein and ACE2 is higher in the BA.2.12.1 complex as compared to BA.4 complex. Due to the overall stability of S protein (BA.2.12.1)-ACE2 complex and increased affinity of the S protein for ACE2, the BA.2.12.1 strain may be more virulent than the BA.4 type strain. The important interactions between the S protein and ACE2 in the complexes of the BA.4 type and the BA.2.12.1 might be employed to develop brand-new inhibitors to combat the recently discovered coronavirus strains

10.6. Bibliography:

[1]. Ludwig, S., and Zarbock, A. Coronaviruses and SARS-CoV-2: A Brief Overview. *Anesthesia & Analgesia*, 131(1): 93-96, 2020. https://doi.org/10.1213%2FANE.0000000000004845

[2]. Duffy, S., Shackelton, L. A., and Holmes, E. C. Rates of evolutionary change in viruses: patterns and determinants. *Nature Reviews Genetics*, 9(4): 267–276, 2008. https://doi.org/10.1038/nrg2323

[3]. Carabelli, A. M., Peacock, T. P., Thorne, L. G., Harvey, W. T., Hughes, J., Peacock, S. J., Barclay, W. S., de Silva, T. I., Towers, G. J., and Robertson, D. L. SARS-CoV-2 variant biology: immune escape, transmission and fitness. *Nature Reviews Microbiology*, 21(3): 162–177, 2023. https://doi.org/10.1038/s41579-022-00841-7

[4]. He, X., He, C., Hong, W., Yang, J., and Wei, X. Research progress in spike mutations of SARS-CoV-2 variants and vaccine development. *Medicinal Research Reviews*, 43(4): 932-971, 2023. https://doi.org/10.1002/med.21941

[5]. Harvey, W. T., Carabelli, A. M., Jackson, B., Gupta, R. K., Thomson, E. C., Harrison, E. M., Ludden, C., Reeve, R., Rambaut, A., Peacock, S. J., and Robertson, D. L. SARS-CoV-2 variants, spike mutations and immune escape. *Nature Reviews Microbiology*, 19(7): 409–424, 2021. https://doi.org/10.1038/s41579-021-00573-0

[6]. Scialo, F., Daniele, A., Amato, F., Pastore, L., Matera, M. G., Cazzola, M., Castaldo, G., and Bianco, A. ACE2: The Major Cell Entry Receptor for SARS-CoV-2. *Lung*, 198: 867-877, 2020. https://doi.org/10.1007/s00408020-00408-4

[7]. Peng, R., Wu, L. A., Wang, Q., Qi, J., and Gao, G. F. Cell entry by SARS-CoV-2. *Trends in Biochemical Sciences*, 46(10): 848-860, 2021. https://doi.org/10.1016/j.tibs.2021.06.001

[8]. Huang, Y., Yang, C., Xu, X. F., and Liu, S. W. Structural and functional properties of SARS-CoV-2 spike protein: potential antivirus drug development for COVID-19. *Acta Pharmacologica Sinica*, 41(9): 1141–1149, 2020. https://doi.org/10.1038/s41401-020-0485-4

[9]. Pathania, A. S., Prathipati, P., Abdul, B. A. A., Chava, S., Katta, S. S., Gupta, S. C., Gangula, P. R., Pandey, M. K., Durden, D. L., Byrareddy, S. N., and Challagundla, K. B. COVID-19 and Cancer Comorbidity: Therapeutic Opportunities and Challenges. *Theranostics*, 11(2): 731-753, 2021. https://doi.org/10.7150/thno.51471

[10]. Islam, F., Dhawan, M., Nafady, M. H., Emran, T. B., Mitra, S., Choudhary, O. P., and Akter, A. Understanding the omicron variant (B.1.1.529) of SARS-CoV-2: Mutational impacts, concerns, and the possible solutions. *Annals of Medicine & Surgery*, 78: 103737, 2022. https://doi.org/10.1016/j.amsu.2022.103737

[11]. Chen, J., He, H., Liu, L., Shang, W., and Guo, Y. Potential immune evasion of the severe acute respiratory syndrome coronavirus 2 Omicron variants. *Frontiers in Immunology*, 13: 1339660, 2024. https://doi.org/10.3389/fimmu.2024.1339660

[12]. Ghimire, D., Han, Y., and Lu, M. Structural Plasticity and Immune Evasion of SARS-CoV-2 Spike Variants. *Viruses*, 14(6): 1255, 2022. https://doi.org/10.3390/v14061255

[13]. Cosar, B., Karagulleoglu, Z. Y., Unal, S., Ince, A. T., Uncuoglu, D. B., Tuncer, G., Kilinc, B. R., Ozkan, Y. E., Ozkoc, H. C., Demir, I. N., Eker, A., Karagoz, F., Simsek, S. Y., Yasar, B., Pala, M., Demir, A., Atak, I. N., Mendi, A. H., Bengi, V. U., Seval, G. C., Altuntas, E. G., Kilic, P., and Demir-Dora, D. SARS-CoV-2 Mutations and their Viral Variants. *Cytokine & Growth Factor Reviews*, 63: 10-22, 2022. https://doi.org/10.1016/j.cytogfr.2021.06.001

[14]. Khateeb, J., Li, Y., and Zhang, H. Emerging SARS-CoV-2 variants of concern and potential intervention approaches. *Critical Care*, 25(244): 1-8, 2021. https://doi.org/10.33263/LIANBS132.096

[15]. Verma, J., and Subbarao, N. Insilico study on the effect of SARS-CoV-2 RBD hotspot mutants' interaction with ACE2 to understand the binding affinity and stability. *Virology*, 561: 107–116, 2021. https://doi.org/10.1016/j.virol.2021.06.009

[16]. Teruel, N., Mailhot, O., and Najmanovich, R. J. Modelling conformational state dynamics and its role on infection for SARS-CoV-2 Spike protein variants. *PLoS Computational Biology*, 17(8): e1009286, 2021. https://doi.org/10.1371/journal.pcbi.1009286

[17]. Noh, J. Y., Jeong, H. W., and Shin, E. C. SARS-CoV-2 mutations, vaccines, and immunity: implication of variants of concern. *Signal Transduction and Targeted Therapy*, 6(1): 203, 2021. https://doi.org/10.1038/s41392-021-00623-2

[18]. Yin, W., Xu, Y., Xu, P., Cao, X., Wu, C., Gu, C., He, X., Wang, X., Huang, S., Yuan, Q., Wu, K., Hu, W., Huang, Z., Liu, J., Wang, Z., Jia, F., Xia, K., Liu, P., Wang, X., Song, B., Zheng, J., Jiang, H., Cheng, X., Jiang, Y., Deng, S.-J., and Xu, H. E. Structures of the Omicron spike trimer with ACE2 and an anti-Omicron antibody. *Science*, 375(6584): 1048-1053, 2022. https://doi.org/10.1126/science.abn8863

[19]. Zhang, Y., Zhang, T., Fang, Y., Liu, J., Ye, Q., and Ding, L. SARS-CoV-2 spike L452R mutation increases Omicron variant fusogenicity and infectivity as well as host glycolysis. *Signal Transduction and Targeted Therapy*, 7(1): 76, 2022. https://doi.org/10.1038/s41392-022-00941-z

[20]. Berman, H. M., Westbrook, J., Feng, Z., Gilliland, G., Bhat, T. N., Weissig, H., Shindyalov, I. N., and Bourne, P. E. The Protein Data Bank. *Nucleic Acids Research*, 28(1): 235-242, 2000. http://doi.org/10.1093/nar/28.1.235

[21]. Pettersen, E. F., Goddard, T. D., Huang, C. C., Couch, G. S., Greenblatt, D. M., Meng, E. C., and Ferrin, T. E. UCSF Chimera-A visualization system for exploratory research and analysis. *Journal of Computational Chemistry*, 25(13): 1605−1612, 2004. http://doi.org/10.1002/jcc.20084

[22]. Dominguez, C., Boelens, R., and Bonvin, A. M. J. J. HADDOCK: A Protein−Protein Docking Approach Based on Biochemical Biophysical Information. *Journal of the American Chemical Society*, 125(7): 1731-1737, 2003. https://doi.org/10.1021/ja026939x

[23]. van Zundert, G. C. P., Rodrigues, J. P. G. L. M., Trellet, M., Schmitz, C., Kastritis, P. L., Karaca, E., Melquiond, A. S. J., van Dijk, M., de Vries, S. J., and Bonvin. A. M. J. J. The HADDOCK2.2 Web Server: User-Friendly Integrative Modeling of Biomolecular Complexes. *Journal of Molecular Biology*, 428(4): 720-725, 2016. https://doi.org/10.1016/j.jmb.2015.09.014

[24]. Gasteiger, E., Gattiker, A., Hoogland, C., Ivanyi, I., Appel, R. D., and Bairoch, A. ExPASY: the proteomics server for in-depth protein knowledge and analysis. *Nucleic Acids Research*, 31(13): 3784-3788, 2003. http://doi.org/10.1093/nar/gkg563

[25]. Sen, T. Z., Jernigan, R. L., Garnier, J., and Kloczkowski, A. Gor V server for protein secondary structure prediction. *Bioinformatics*, 21(11): 2787–2788, 2005. https://doi.org/10.1093/bioinformatics/bti408

[26]. Sievers, F., and Higgins, D. G. Clustal Omega for making accurate alignments of many protein sequences. *Protein Science*, 27(1): 135-145, 2018. http://doi.org/10.1002/pro.3290

[27]. Xue, B., Dunbrack, R. L., Williams, R. W., Dunker, A. K., and Uversky, V. N. PONDR-FIT: A meta-predictor of intrinsically disordered amino acids. *Biochimica et Biophysica Acta (BBA)-Proteins and Proteomics*, 1804(4): 996-1010, 2010. http://doi.org/10.1016/j.bbapap.2010.01.011

[28]. Case, D. A., Cheatham III, T. E., Darden, T., Gohlke, H., Luo, R., Merz Jr., K. M., Onufriev, A., Simmerling, C., Wang, B., and Woods, R. J. The Amber biomolecular simulation programs. *Journal of Computational Chemistry*, 26(16): 1668-1688, 2005. https://doi.org/10.1002/jcc.20290

[29]. Tian, C., Kasavajhala, K., Belfon, K. A. A., Raguette, L., Huang, H., Migues, A. N., Bickel, J., Wang, Y., Pincay, J., Wu, Q., and Simmerling, C. ff19SB: Amino-Acid-Specific Protein Backbone Parameters Trained against Quantum Mechanics Energy Surfaces in Solution. *Journal of Chemical Theory and Computation*, 16(1): 528-552, 2019. https://doi.org/10.1021/acs.jctc.9b00591

[30]. Jorgensen, W. L., Chandrasekhar, J., Madura, J. D., Impey, R. W., and Klein, M. L. Comparison of simple potential functions for simulating liquid water. *The Journal of Chemical Physics*, 79(2): 926−935, 1983. https://doi.org/10.1063/1.445869

[31]. Salomon-Ferrer, R., Götz, A. W., Poole, D., Le Grand, S., and Walker, R. C. Routine Microsecond Molecular Dynamics Simulations with AMBER on GPUs. 2. Explicit Solvent Particle Mesh Ewald. *Journal of Chemical Theory and Computation*, 9(9): 3878-3888, 2013. https://doi.org/10.1021/ct400314y

[32]. Darden, T., York, D., and Pedersen, L. Particle mesh Ewald: An N·log(N) method for Ewald sums in large systems. *Journal of Chemical Physics*, 98: 10089, 1993. https://doi.org/10.1063/1.464397

[33]. Krautler V, Gunsteren W.F.V., and Hunenberger P.H. A fast SHAKE: Algorithm to solve distance constraint equations for small molecules in molecular dynamics simulations. *Journal of Computational Chemistry,* 22: 501-508, 2001. http://dx.doi.org/10.1002/1096-987X(20010415)22:53.0.CO;2-V

[34]. Berendsen, H. J. C., Postma, J. P. M., van Gunsteren, W. F., DiNola, A., and Haak, J. R. Molecular dynamics with coupling to an external bath. *The Journal of Chemical Physics*, 81(8): 3684-3690, 1984. https://doi.org/10.1063/1.448118

[35]. Laskowski, R. A., Hutchinson, E. G., Michie, A. D., Wallace, A. C., Jones, M. L., and Thornton, J. M. PDBsum: a web-based database of summaries and analyses of all PDB structures. *Trends in Biochemical Sciences*, 22(12): 488-490, 1997. https://doi.org/10.1016/s0968-0004(97)01140-7

[36]. Chen, F., Liu, H., Sun, H., Pan, P., Li, Y., Li, D., and Hou, T. Assessing the performance of the MM/PBSA and MM/GBSA methods. 6. Capability to predict protein–protein binding free energies and re-rank binding poses generated by protein–protein docking. *Physical Chemistry Chemical Physics*, 18(32): 22129-22139, 2016. https://doi.org/10.1039/C6CP03670H

[37]. Genheden, S., and Ryde, U. The MM/PBSA and MM/GBSA methods to estimate ligand-binding affinities. *Expert Opinion on Drug Discovery*, 10(5): 449-461, 2015. https://doi.org/10.1517/17460441.2015.1032936

[38]. Sun, H., Duan, L., Chen, F., Liu, H., Wang, Z., Pan, P., Zhu, F., Zhang, J. Z. H., and Hou, T. Assessing the performance of MM/PBSA and MM/GBSA methods. 7. Entropy effects on the performance of end-point binding free energy calculation approaches. *Physical Chemistry Chemical Physics*, 20(21): 14450-14460, 2018. https://doi.org/10.1039/C7CP07623A

[39]. Tian, S., Ji, C., and Zhang, J. Z. H. Molecular basis of SMAC–XIAP binding and the effect of electrostatic polarization. *Journal of Biomolecular Structure and Dynamics*, 39(2): 743-752, 2021. https://doi.org/10.1080/07391102.2020.1713892

[40]. Wan, Y., Guan, S., Qian, M., Huang, H., Han, F., Wang, S., and Zhang, H. Structural basis of fullerene derivatives as novel potent inhibitors of protein acetylcholinesterase without catalytic active site interaction: insight into the inhibitory mechanism through molecular modeling studies. *Journal of Biomolecular Structure and Dynamics*, 38(2): 410-425, 2020. https://doi.org/10.1080/07391102.2019.1576543

[41]. Wang, E., Sun, H., Wang, J., Wang, Z., Liu, H., Zhang, J. Z. H., and Hou, T. End-Point Binding Free Energy Calculation with MM/PBSA and MM/GBSA: Strategies and Applications in Drug Design. *Chemical Reviews*, 119(16): 9478-9508, 2019. https://doi.org/10.1021/acs.chemrev.9b00055

[42]. Das, C., Das, D., and Mattaparthi, V. S. K. Effect of Mutations in the SARS-CoV-2 Spike RBD Region of Delta and Delta-Plus Variants on its Interaction with ACE2 Receptor Protein. *Letters in Applied NanoBioScience*, 12(4): 118, 2023. https://doi.org/10.33263/LIANBS124.118

[43]. Das, C., Hazarika, P. J., Deb, A., Joshi, P., Das, D., and Mattaparthi, V. S. K. Effect of Double Mutation (L452R and E484Q) in RBD of Spike Protein on its Interaction with ACE2 Receptor Protein. *Biointerface Research in Applied Chemistry*, 13(1): 97, 2023. https://doi.org/10.33263/BRIAC131.097

[43]. Das, C., Das, D., and Mattaparthi, V. S. K. Computational Investigation on the Efficiency of Small Molecule Inhibitors Identified from Indian Spices against SARS-CoV-2 Mpro. *Biointerface Research in Applied Chemistry*, 13(3): 235, 2023. https://doi.org/10.33263/BRIAC133.235

[44]. Das, C., and Mattaparthi, V. S. K. Impact of Mutations in the SARS-CoV-2 Spike RBD Region of BA1 and BA2 Variants on its Interaction with ACE2 Receptor Protein. *Biointerface Research In Applied Chemistry*, 13(4): 358, 2023. https://doi.org/10.33263/BRIAC134.358